Article

Formation and Characterization of the Hexanuclear Platinum Cluster [Pt(□-PBu)(CO)](CFSO) through Structural, Electrochemical, and Computational Analyses

Fabrizia Fabrizi de Biani, Andrea Ienco, Franco Laschi, Piero Leoni, Fabio Marchetti, Lorella Marchetti, Carlo Mealli, and Piero Zanello

J. Am. Chem. Soc., **2005**, 127 (9), 3076-3089• DOI: 10.1021/ja043626o • Publication Date (Web): 12 February 2005

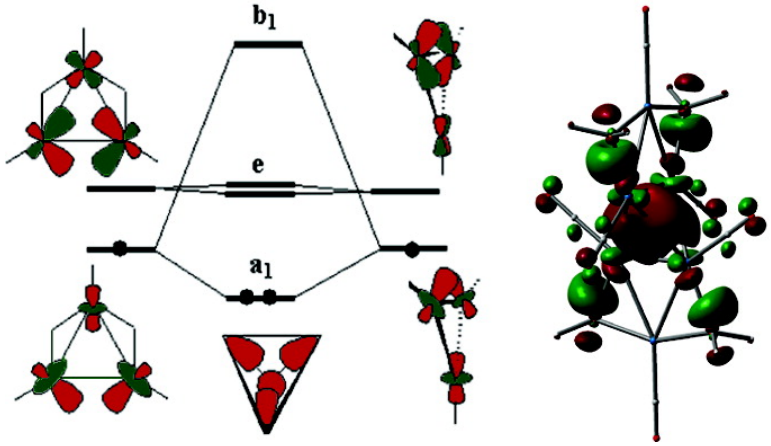

More About This Article

Additional resources and features associated with this article are available within the HTML version:

- Supporting Information
- Links to the 4 articles that cite this article, as of the time of this article download
- Access to high resolution figures
- Links to articles and content related to this article
- Copyright permission to reproduce figures and/or text from this article

View the Full Text HTML

J|A|C|S
ARTICLES
Published on Web 02/12/2005

Formation and Characterization of the Hexanuclear Platinum Cluster $[Pt_6(\mu\text{-}PBu^t_2)_4(CO)_6](CF_3SO_3)_2$ through Structural, Electrochemical, and Computational Analyses

Fabrizia Fabrizi de Biani,[#] Andrea Ienco,[⊥] Franco Laschi,[#] Piero Leoni,*[,†] Fabio Marchetti,[†] Lorella Marchetti,[†] Carlo Mealli,*[,⊥] and Piero Zanello*[,#]

Contribution from the Dipartimento di Chimica dell'Università di Siena, Via A. Moro, I-53100 Siena, Italy, Dipartimento di Chimica e Chimica Industriale dell'Università di Pisa, Via Risorgimento 35, I-56126 Pisa, Italy, and Istituto di Chimica dei Composti Organometallici (ICCOM) del CNR, Via Madonna del Piano, I-50019 Sesto Fiorentino (Fi), Italy

Received October 20, 2004; E-mail: leoni@dcci.unipi.it (P.L.); mealli@iccom.cnr.it (C.M.); zanello@unisi.it (P.Z.)

Abstract: The reaction between equimolar amounts of $Pt_3(\mu\text{-}PBu^t_2)_3(H)(CO)_2$, **$Pt_3H$**, and CF_3SO_3H under CO atmosphere affords the triangular species $[Pt_3(\mu\text{-}PBu^t_2)_3(CO)_3]X$, **$[Pt_3(CO)_3^+]X$** (X = $CF_3SO_3^-$), characterized by X-ray crystallography, or in an excess of acid, $[Pt_6(\mu\text{-}PBu^t_2)_4(CO)_6]X_2$, **$[Pt_6^{2+}]X_2$**. Structural determination shows the latter to be a rare hexanuclear cluster with a Pt_4 tetrahedral core formed by joining the unbridged sides of two orthogonal Pt_3 triangles. The dication **Pt_6^{2+}** features also extensive redox properties as it undergoes two reversible one-electron reductions to the congeners $[Pt_6(\mu\text{-}PBu^t_2)_4(CO)_6]^+$ (**Pt_6^+**, $E_{1/2} = -0.27$ V) and $Pt_6(\mu\text{-}PBu^t_2)_4(CO)_6$ (**Pt_6**, $E_{1/2} = -0.54$ V) and a further quasi-reversible two-electron reduction to the unstable dianion **Pt_6^{2-}** ($E_{1/2} = -1.72$ V). The stable radical (**Pt_6^+**) and diamagnetic (**Pt_6**) species are also formed via chemical methods by using 1 or 2 equiv of Cp_2Co, respectively; further reduction of **Pt_6^{2+}** causes fast decomposition. The chloride derivatives $[Pt_6(\mu\text{-}PBu^t_2)_4(CO)_5Cl]X$, **$(Pt_6Cl^+)X$**, and $Pt_6(\mu\text{-}PBu^t_2)_4(CO)_4Cl_2$, **$Pt_6Cl_2$**, observed as side-products in some electrochemical experiments, were prepared independently. The reaction leading to **$Pt_3(CO)_3^+$** has been analyzed with DFT methods, and identification of key intermediates allows outlining the reaction mechanism. Moreover, calculations for the whole series **$Pt_6^{2+} \rightarrow Pt_6^{2-}$** afford the otherwise unknown structures of the reduced derivatives. While the primary geometry is maintained by increasing electron population, the system undergoes progressive and concerted out-of-plane rotation of the four phosphido bridges (from D_{2d} to D_2 symmetry). The bonding at the central Pt_4 tetrahedron of the hexanuclear clusters (an example of 4c-2e$^-$ inorganic tetrahedral aromaticity in **Pt_6^{2+}**) is explained in simple MO terms.

Introduction

Unlike rather common trinuclear clusters, hexanuclear platinum species are exceedingly rare. Trigonal prismatic and octahedral polyhedra may be considered as being derived from the stacking of two triangles in an eclipsed or in a staggered way. The two structural types are exemplified by the $[Pt_6(\mu\text{-}CO)_6(CO)_6]^{2-}$ anion[1] and by the $[Pt_6(CO)_6(\mu\text{-dppm})_3]^{2+}$ cation, respectively.[2] To the best of our knowledge, no other hexaplatinum cluster has been authenticated by X-ray crystallography, including the synthesized species $[Pt_6(\mu\text{-}SO_2)_3(CNXyl)_9]$ which is only suggested to have a capped trigonal bipyramidal structure.[3] The limited number of known Pt_6 clusters is likely due to steric problems, which prevent the superimposition of two sterically hindered $[Pt_3(\mu\text{-}L)_3(L')_3]$ units. For instance, this factor seems crucial for uncharged or cationic systems with *tert*-butylphoshido bridges, such as $Pt_3(\mu\text{-}PBu^t_2)_3(CO)_2(H)$, **$Pt_3H$**,[4] or $[Pt_3(\mu\text{-}PBu^t_2)_3(L)_3]^+$.[5] An alternative way of coupling two Pt_3 triangular cores is that followed by the mixed-metal anions, $[Fe_3Pt_3(CO)_{15}]^-$, which contain $Fe(CO)_4$ bridges between Pt(CO) units. The conversion into the decanuclear product, $[Fe_4Pt_6(CO)_{22}]^{2-}$,[6] was suggested to proceed through the loss of an $Fe(CO)_4$ fragment per triangular unit and the orthogonal condensation of two trapezoidal $[Fe_2Pt_3(CO)_{11}]^-$ anions (Scheme 1). A tetrahedral platinum core is thus originated.

Scheme 1

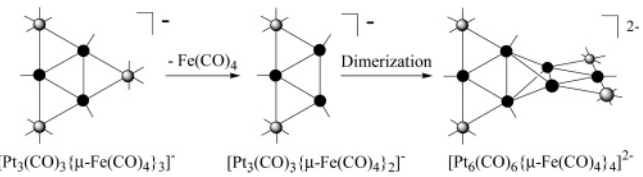

[#] Università di Siena.
[†] Università di Pisa.
[⊥] ICCOM.

(1) Calabrese, J. C.; Dahl, L. F.; Chini, P.; Longoni, G.; Martinengo, S. *J. Am. Chem. Soc.* **1974**, *96*, 2614.
(2) Hao, L.; Spivak, G. J.; Xiao, J.; Vittal, J. J.; Puddephatt, R. J. *J. Am. Chem. Soc.* **1995**, *117*, 7011.
(3) Haggitt, J. L.; Mingos, D. M. P. *J. Chem. Soc., Dalton Trans.* **1994**, 1013.
(4) Leoni, P.; Manetti, S.; Pasquali, M.; Albinati, A. *Inorg. Chem.* **1996**, *35*, 6045.
(5) Leoni, P.; Marchetti, F.; Pasquali, M.; Marchetti, L.; Albinati, A. *Organometallics* **2002**, *21*, 2176.

10.1021/ja043626o CCC: $30.25

The precursor of the chemistry reported in this paper is the triangular cluster **Pt_3H**, and for the reader's convenience, we anticipate in Scheme 2 a map of the various reaction paths (a−i), which are referenced throughout the paper.

Scheme 2. Possible Pathways for the Formation of **$Pt_3(CO)_3^+$** and **Pt_6^{2+}** (Methyl Groups of the *t*-Butyls are Omitted for Clarity)[a]

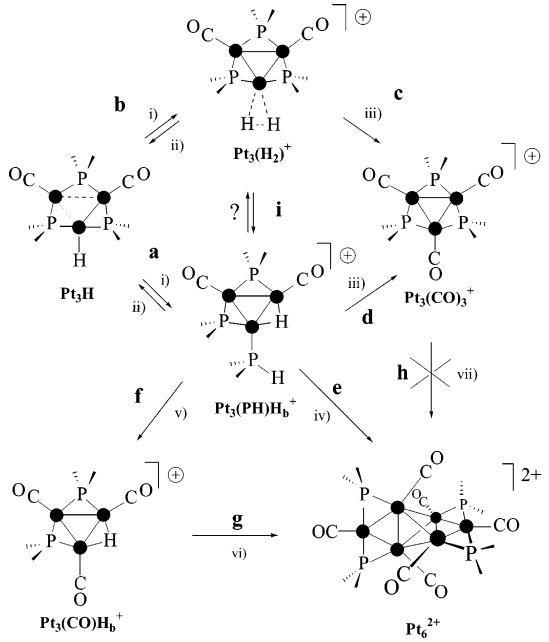

[a] (i) H^+; (ii) B, $-BH^+$; (iii) CO, $-H_2$; (iv) $H^+_{(xs)}$, CO, $-H_2$, $-[PBu^t_2H_2]^+$; (v) $H^+_{(xs)}$, CO, $-[PBu^t_2H_2]^+$; (vi) $-H_2$; (vii) $H^+_{(xs)}$, CO.

As an already established result, protonation of **Pt_3H** with triflic acid under N_2 converts one of the bulky phosphido bridges into a terminal secondary phosphine, and the species [Pt$_3$(μ-PBu$^t_2$)$_2$(μ-H)(PBu$^t_2$H)(CO)$_2$]X, **[$Pt_3(PH)H_b^+$]X**, is reversibly formed (equilibrium a).[7] The latter cation reacts with CO to give the trisphosphido species [Pt$_3$(μ-PBu$^t_2$)$_3$(CO)$_3$]X, **[$Pt_3(CO)_3^+$]X**, either through a direct path (d) or through the Pt-η^2H$_2$ intermediate, **$Pt_3(H_2)^+$** (paths i + c). In principle, **$Pt_3(H_2)^+$** can also be the species that connects **Pt_3H** with **$Pt_3(PH)H_b^+$** (paths b + c). The hexanuclear cluster [Pt$_6$(μ-PBu$^t_2$)$_4$(CO)$_6$]X$_2$, **(Pt_6^{2+})X_2**, is obtained when the carbonylation of **$Pt_3(PH)H_b^+$** is carried out in excess of triflic acid (path e). In investigating the formation of **Pt_6^{2+}**, we find no direct link with **$Pt_3(CO)_3^+$** (path h). Conversely, it may not be excluded that the reaction proceeds through the intermediate **$Pt_3(CO)H_b^+$** (paths f + g), which is unobserved despite its close similarity to **$Pt_3(PH)H_b^+$**.

The **Pt_6^{2+}** cluster is shown by X-ray diffraction[8] to have a dibridged tetrahedral Pt$_6$ core similar to the one observed in [Fe$_4$Pt$_6$(CO)$_{22}$]$^{2-}$, and its structural features will be illustrated in detail together with those of **$Pt_3(CO)_3^+$**. Moreover, this paper presents exhaustive chemical, electrochemical, and computational results. In particular, several redox derivatives of **Pt_6^{2+}**, observed via electrochemical methods and in some cases achieved via chemical synthesis, have been structurally characterized with DFT optimizations.

Finally, species, such as **$Pt_3(CO)_3^+$** and **Pt_6^{2+}**, have already been shown[9] to have a role as building blocks in the construction of rigid-rod or dendrimeric structures with potential technological applications. The usage of coordination or organometallic frameworks to construct new materials, which can extend in one, two, or three dimensions on a nanometric scale, is a topic attracting enormous interest in the recent literature.[10] For instance, directional assembly of ordered metal−organic frameworks (MOF) is challenging for their potential applications in the reversible storage/release of gases.[11] On the other hand, cluster-containing assemblies are relatively unexplored, and the examples of structurally characterized compounds with two[12] or more[13] cluster units are still very limited.[14] It is noteworthy that metal clusters, such as the present units, can be directionally connected by means of conjugated or insulating spacers, and the peculiar redox behavior of the units could be locally maintained or even enhanced upon their assembly. Part of this work has been briefly communicated.[8]

Results and Discussion

The protonation of **Pt_3H** with triflic acid (path a) occurs at one of the two CO-coordinated metal atoms and is followed by the formation of a P−H bond between the bridging phosphido

(6) Longoni, G.; Manassero, M.; Sansoni, M. *J. Am. Chem. Soc.* **1980**, *102*, 7973.
(7) Fortunelli, A.; Leoni, P.; Marchetti, L.; Pasquali, M.; Sbrana, F.; Selmi, M. *Inorg. Chem.* **2001**, *40*, 3055.
(8) Leoni, P.; Marchetti, F.; Marchetti, L.; Pasquali, M.; Quaglierini, S. *Angew. Chem., Int. Ed.* **2001**, *40*, 3617.
(9) (a) Albinati, A.; Leoni, P.; Marchetti, L.; Rizzato, S. *Angew. Chem., Int. Ed.* **2003**, *42*, 5990. (b) Leoni, P.; Marchetti, F.; Marchetti, L.; Pasquali, M. *Chem. Commun.* **2003**, 2372.
(10) (a) Choi, M.-S.; Yamazaki, T.; Yamazaki, I.; Aida, T. *Angew. Chem., Int. Ed.* **2004**, *43*, 150. (b) Hof, F.; Craig, S. L.; Nuckolls, C.; Rebeck, J., Jr. *Angew. Chem., Int. Ed.* **2002**, *41*, 1488. (c) Seidel, S. R.; Stang, P. J. *Acc. Chem. Res.* **2002**, *35*, 972. (d) Swiegers, G. F.; Malefetse, T. J. *Chem. Rev.* **2000**, *100*, 3483. (e) Müller, A.; Kögerler, P. *Coord. Chem. Rev.* **1999**, *182*, 3. (f) Schwab, P. F. H.; Levin, M. D.; Michl, J. *Chem. Rev.* **1999**, *99*, 1863. (g) Newkome, G. R.; He, E.; Moorefield, C. N. *Chem. Rev.* **1999**, *99*, 1689. (h) Robertson, N.; McGowan, C. A. *Chem. Soc. Rev.* **2003**, *32*, 96. (i) Janiak, C. *Dalton Trans.* **2003**, 2781. (j) Jimenez-Molero, M. C.; Dietrich-Buchecker, C.; Sauvage, J.-P. *Chem. Commun.* **2003**, 1613. (k) Molecular Machines Special Issue *Acc. Chem. Res.* **2001**, *34*, 409−522. (l) Holliday, B. J.; Mirkin, C. A. *Angew. Chem., Int. Ed.* **2001**, *40*, 2022. (m) Gust, D.; Moore, T. A.; Moore, A. L. *Acc. Chem. Res.* **2001**, *34*, 40. (n) Balzani, V.; Credi, A.; Raymo, F. M.; Stoddart, J. F. *Angew. Chem., Int. Ed.* **2000**, *39*, 3349. (o) Szafert, S.; Gladysz, J. A. *Chem. Rev.* **2003**, *103*, 4175. (p) Stott, T. L.; Wolf, M. O. *Coord. Chem. Rev.* **2003**, *246*, 89. (q) Paul, F.; Lapinte, C. *Coord. Chem. Rev.* **1998**, *178*−*180*, 431. (r) Xu, G.-L.; Zou, G.; Ni, Y.-H.; DeRosa, M. C.; Crutchley, R. J.; Ren, T. *J. Am. Chem. Soc.* **2003**, *125*, 10057. (s) Cotton, F. A.; Lin, C.; Murillo, C. A. *Acc. Chem. Res.* **2001**, *34*, 759. (t) Chisholm, M. H. *Acc. Chem. Res.* **2000**, *33*, 53. (u) Wong, K.-T.; Lehn, J.-M.; Peng, S.-M.; Lee, G.-H. *Chem. Commun.* **2000**, 2259. (v) Irwin, M. J.; Jia, G.; Vittal, J. J.; Puddephatt, R. J. *Organometallics* **1996**, *15*, 5321.
(11) Rosi, N. L.; Eckert, J.; Eddaoudi, M.; Vodak, D. T.; Kim, J.; O'Keeffe, M.; Yaghi, O. M. *Science* **2003**, *300*, 1127.
(12) (a) Choualeb, A.; Braunstein, P.; Rosé, J.; Welter, R. *Inorg. Chem.* **2004**, *43*, 57. (b) Roland, B. K.; Selby, H. D.; Cole, J. R.; Zheng, Z. *Dalton Trans.* **2003**, 4307. (c) Akita, M.; Sakurai, A.; Chung, M.-C.; Moro-oka, Y. *J. Organomet. Chem.* **2003**, *670*, 2. (d) Zhu, B.-H.; Hu, B.; Zhang, W.-Q.; Zhang, Y.-H.; Yin, Y.-Q.; Sun, J. *J. Organomet. Chem.* **2003**, *681*, 275. (e) Bruce, M. I.; Smith, M. E.; Zaitseva, N. N.; Skelton, B. W.; White, A. H. *J. Organomet. Chem.* **2003**, *670*, 170. (f) Westmeyer, M. D.; Massa, M. A.; Rauchfuss, T. B.; Wilson, S. R. *J. Am. Chem. Soc.* **1998**, *120*, 114. (g) Hui, J. W.-S.; Wong, W.-T. *J. Chem. Soc., Dalton Trans.* **1997**, 2445. (h) Imhof, D.; Burkhardt, U.; Dahmen, K.-H.; Joho, F.; Nesper, R. *Inorg. Chem.* **1997**, *36*, 1813. (i) Yam, V. W.-W.; Fung, W. K.-M.; Cheung, K.-K. *Chem. Commun.* **1997**, 963. (j) Osella, D.; Milone, L.; Nervi, C.; Ravera, M. *J. Organomet. Chem.* **1995**, *488*, 1. (k) Jensen, M. P.; Phillips, D. A.; Sabat, M.; Shriver, D. F. *Organometallics* **1992**, *11*, 1859. (l) Worth, G. H.; Robinson, B. H. *Organometallics* **1992**, *11*, 501. (m) Furuya, F. R.; Miller, L. L.; Hainfeld, J. F.; Christopfel, W. C.; Kenny, P. W. *J. Am. Chem. Soc.* **1988**, *110*, 641.
(13) (a) Humphrey, M. G. *Macromol. Symp.* **2004**, *209*, 1. (b) Notaras, E. G. A.; Lucas, N. T.; Humphrey, M. G.; Willis, A. C.; Rae, A. D. *Organometallics* **2003**, *22*, 3659. (c) Roland, B. K.; Carter, C.; Zheng, Z. *J. Am. Chem. Soc.* **2002**, *124*, 6234. (d) Feeder, N.; Geng, J.; Goh, P. G.; Johnson, B. F. G.; Martin, C. M.; Shepard, D. S.; Zhou, W. *Angew. Chem., Int. Ed.* **2000**, *39*, 1661. (e) Alonso, E.; Astruc, D. *J. Am. Chem. Soc.* **2000**, *122*, 3222. (f) Benito, M.; Rossell, O.; Seco, M.; Segalés, G. *Organometallics* **1999**, *18*, 5191. (g) Lei, X.; Wolf, E. E.; Fehlner, T. P. *Eur. J. Inorg. Chem.* **1998**, 1835. (h) Ritter, U.; Winkhofer, N.; Murugavel, R.; Voigt, A.; Stalke, D.; Roesky, H. W. *J. Am. Chem. Soc.* **1996**, *118*, 8580.

and the pre-existing hydride ligand. In the cationic product, $\mathbf{Pt_3(PH)H_b^+}$,[7,15] the added proton occupies a bridging position. The reduced steric hindrance between the related metal atoms should further diminish if the terminal secondary phosphine was substituted with a carbonyl ligand. Therefore, we reacted $\mathbf{[Pt_3(PH)H_b^+]X}$ with CO, expecting the formation of the bisphosphido-bridged hydride $[Pt_3(\mu\text{-}PBu^t_2)_2(\mu\text{-}H)(CO)_3]X$, $\mathbf{[Pt_3(CO)H_b^+]X}$ (path f). Surprisingly, evolution of molecular hydrogen was observed, followed by the quantitative formation of green crystals. After spectroscopic[16] and single-crystal X-ray characterization (vide infra), the latter was identified as the trisphosphido-bridged compound $[Pt_3(\mu\text{-}PBu^t_2)_3(CO)_3]X$, $\mathbf{[Pt_3(CO)_3^+]X}$. The latter forms quantitatively (together with H_2) also by direct reaction of $\mathbf{Pt_3H}$ with an equimolar amount of triflic acid under 1 atm of carbon monoxide.

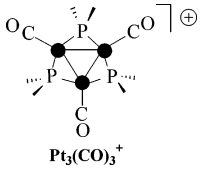

$\mathbf{Pt_3(CO)_3^+}$

The formation of hydrogen upon protonation of a neutral metal hydride complex is a well-known organometallic reaction.[17] As depicted in eq 1, the process may involve the M−H bond or the metal itself, with the formation of a dihydride or a nonclassical dihydrogen complex, while the evolution of H_2 is favored by the addition of another ligand (L′).

$$L_nM-H \xrightarrow{H^+} L_nM(H)_2^+ \text{ or } L_nM(H_2)^+ \xrightarrow[-H_2]{L'} L_nM-L'^+ \quad (1)$$

This could be the case (steps b + c) for the conversion of the hydride $\mathbf{Pt_3H}$ into cation $\mathbf{Pt_3(CO)_3^+}$, which could involve a classical or nonclassical dihydrogen species $[Pt_3(\mu\text{-}PBu^t_2)_3(CO)_2(\eta^2\text{-}H_2)]X$, $\mathbf{[Pt_3(H_2)^+]X}$, although no such intermediate has ever been detected experimentally.

On the other hand, $\mathbf{Pt_3(PH)H_b^+}$ can be considered the key intermediate in the overall a + d path since it is the unique protonation product of $\mathbf{Pt_3H}$ and readily generates $\mathbf{Pt_3(CO)_3^+}$. Thus, the role of CO, after the formation of $\mathbf{Pt_3(PH)H_b^+}$, is that of inducing P−H scission and H_2 elimination. In this respect, it is worth mentioning that, in N_2 rather than in CO atmosphere, the treatment of $\mathbf{Pt_3H}$ with CF_3SO_3D selectively adds deuterium to the bridging position (cation $\mathbf{Pt_3(PH)D_b^+}$, as shown eq 2), and no rapid H/D scrambling is observed.[7] These aspects will be re-examined also by computational methods (vide infra).

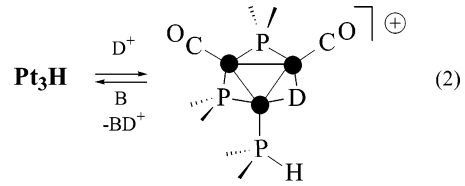

$\mathbf{Pt_3(PH)D_b^+}$ (2)

Molecular Structure of $[Pt_3(\mu\text{-}PBu^t_2)_3(CO)_3]X$, $[Pt_3(CO)_3^+]X$. Single crystals were grown using a solvent mixture of acetone and Et_2O. An ORTEP diagram of the structure of cation $\mathbf{Pt_3(CO)_3^+}$ is shown in Figure 1, and significant bond distances and angles are listed in Table 1.

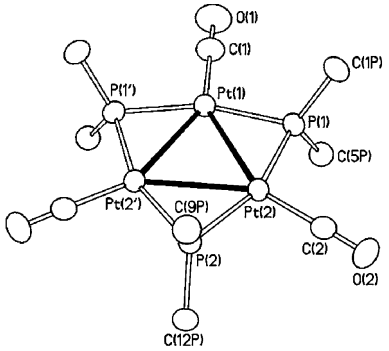

Figure 1. Molecular structure of cation $[Pt_3(\mu\text{-}PBu^t_2)_3(CO)_3]^+$. The methyl groups are omitted for the sake of clarity. Thermal ellipsoids are at 30% probability. The apexes in the atom labels have the same meaning as in Table 1.

Table 1. Bond Lengths (Å) and Angles (deg) around the Metal for $\mathbf{Pt_3(CO)_3^+}$[a]

Pt(1)−Pt(2)	2.961(1)	P(1)−C(1P)	1.85(2)
Pt(2)−Pt(2′)	2.982(1)	P(1)−C(5P)	1.87(2)
Pt(1)−P(1)	2.307(4)	P(2)−C(9P)	1.85(2)
Pt(2)−P(1)	2.314(4)	P(2)−C(12P)	1.89(2)
Pt(2)−P(2)	2.308(5)	C(1)−O(1)	1.11(3)
Pt(1)−C(1)	1.87(2)	C(2)−O(2)	1.15(2)
Pt(2)−C(2)	1.83(2)		
Pt(2)−Pt(1)−Pt(2′)	60.49(3)	P(2)−Pt(2)−Pt(1)	109.4(1)
Pt(1)−Pt(2)−Pt(2′)	59.76(2)	P(1)−Pt(1)−P(1′)	160.8(2)
C(1)−Pt(1)−P(1)	99.6(1)	P(1)−Pt(2)−P(2)	159.4(2)
C(2)−Pt(2)−P(1)	100.5(5)	Pt(1)−P(1)−Pt(2)	79.7(1)
C(2)−Pt(2)−P(2)	100.1(5)	Pt(2)−P(2)−Pt(2′)	80.5(2)
C(1)−Pt(1)−Pt(2)	149.6(1)	C(1P)−P(1)−Pt(1)	114.6(6)
C(2)−Pt(2)−Pt(1)	150.5(5)	C(5P)−P(1)−Pt(1)	114.7(6)
C(2)−Pt(2)−Pt(2′)	149.6(5)	C(1P)−P(1)−Pt(2)	115.0(7)
P(1)−Pt(1)−Pt(2)	50.3(1)	C(5P)−P(1)−Pt(2)	113.0(6)
P(1)−Pt(2)−Pt(1)	50.1(1)	C(1P)−P(1)−C(5P)	115.1(8)
P(2)−Pt(2)−Pt(2′)	49.7(1)	C(9P)−P(2)−Pt(2)	113.3(6)
P(1)−Pt(1)−Pt(2′)	110.7(1)	C(12P)−P(2)−Pt(2)	114.3(6)
P(1)−Pt(2)−Pt(2′)	109.8(1)	C(9P)−P(2)−C(12P)	116.1(11)

[a] Symmetry transformations used to generate equivalent atoms: $' = x, {}^1/_2 - y, z$.

(14) The structures cited in refs 12 and 13 generally contain low-valent carbonyl clusters. Related works describe the preparation of polymers or extended 3D coordination or hydrogen-bonded networks, mainly constructed with medium-valent halide or calchogenide clusters: (a) Roland, B. K.; Selby, H. D.; Cole, J. R.; Zheng, Z. *Dalton Trans.* **2003**, 4307. (b) Yan, B.; Zhou, H.; Lachgar, A. *Inorg. Chem.* **2003**, *42*, 8818. (c) Liu, C. W.; Hung, C.-M.; Haia, H.-C.; Liaw, B.-J.; Liou, L.-S.; Tsai, Y.-F.; Wang, J.-C. *Chem. Commun.* **2003**, 976. (d) Cordier, S.; Gulo, F.; Roisnel, T.; Gautier, R.; le Guennic, B.; Halet, J. F.; Perrin, C. *Inorg. Chem.* **2003**, *42*, 8320. (e) Jin, S.; DiSalvo, F. J. *Chem. Mater.* **2002**, *14*, 3448. (f) Bennett, M. V.; Beauvais, L. G.; Shores, M. P.; Long, J. R. *J. Am. Chem. Soc.* **2001**, *123*, 8022. (g) Kim, Y.; Park, S.-M.; Nam, W.; Kim, S.-J. *Chem. Commun.* **2001**, 1470. (h) Nakajima, T.; Ishiguro, A.; Wakatsuki, Y. *Angew. Chem., Int. Ed.* **2001**, *40*, 1066. (i) Prokopuk, N.; Weinert, C. S.; Siska, D. P.; Stern, C. L.; Shriver, D. F. *Angew. Chem., Int. Ed.* **2000**, *39*, 3312. (j) Naumov, N. G.; Virovets, A. V.; Sokolov, M. N.; Artemkina, S. B.; Fedorov, V. E. *Angew. Chem., Int. Ed.* **1998**, *37*, 1943. (k) Bradford, A. M.; Kristof, E.; Rashidi, M.; Yang, D.-S.; Payne, N. C.; Puddephatt, R. J. *Inorg. Chem.* **1994**, *33*, 2355.

(15) The remarkable steric hindrance in $\mathbf{Pt_3H}$ allowed us to observe a thermally unstable intermediate. On the basis of its NMR features and of a theoretical study,[7] this was suggested to be the Pt−CO···H−OTf hydrogen-bonded adduct, $\mathbf{Pt_3H{\cdot}HOTf}$.

(16) The cation $\mathbf{Pt_3(CO)_3^+}$ has been obtained as the PF_6^- salt by a different synthetic procedure; details of its IR and NMR characterization have been discussed in ref 5.

(17) (a) Papish, E. T.; Rix, F. C.; Spetseris, N.; Norton, J. R.; Williams, R. D. *J. Am. Chem. Soc.* **2000**, *122*, 12235. (b) Bartucz, T. Y.; Golombek, A.; Lough, A. J.; Maltby, P. A.; Morris, R. H.; Ramachandran, R.; Schlaf, M. *Inorg. Chem.* **1998**, *37*, 1555. (c) Kuhlman, R. *Coord. Chem. Rev.* **1997**, *167*, 205. (d) Quadrelli, E. A.; Kraatz, H.-B.; Poli, R. *Inorg. Chem.* **1996**, *35*, 5154. (e) Bullock, R. M.; Song, J.-S.; Szalda, D. J. *Organometallics* **1996**, *15*, 2504.

The complex cation contains a crystallographic mirror plane through the atoms Pt(1), P(2), C(9P), and C(12P) and exhibits a nearly equilateral triangular (quasi-D_{3h}) structure. Trinuclear clusters of general formula $[Pt_3(\mu\text{-}PR_2)_3(L)_3]^+$, which contain 44 valence electrons, can exhibit a structural dichotomy which has been fully ascertained for the uncharged complex, $[Pt_3(\mu\text{-}PPh_2)_3(PPh_3)_2Ph]$.[18] One isomer of this complex has two short and one elongated Pt−Pt separations of 2.76 and 3.59 Å, respectively, while the second isomer has three equally long Pt−Pt bonds of about 2.99 Å (average value). The latter situation is observed in cation $\mathbf{Pt_3(CO)_3}^+$ since the Pt−Pt−Pt angles are approximately 60° [Pt1−Pt2−Pt2′ = 59.75(2)° and Pt2−Pt1−Pt2′ = 60.49(3)°] and the intermetallic separations are 2.960(1) and 2.983(1) Å for the independent Pt1−Pt2 and Pt2−Pt2′ bonds, respectively. These values are also consistent with those in the $[Pt_3(\mu\text{-}PPh_2)_3(PPh_3)_2(Si(OSiMe_3)_3]$[19] structure (average Pt−Pt distance of 2.974 Å). An intermediate situation is found between the two previously indicated limits in another 44e$^-$ complex, namely, $[Pt_3(\mu\text{-}PBu^t_2)_3(CNBu^t)_2(H)]$,[5] which has two shorter Pt−Pt sides of 2.91 Å (average) and a longer one of 3.17 Å, opposite to the hydride ligand. Although the distance is significantly stretched, residual M−M bonding is not to be excluded. Finally, it is worth recalling that about 20 structures featuring triply bridged Pt_3 framework and a 42 electron count are deposited in the Cambridge Structural Database.[20] The bridges are of quite different nature, but the metal skeleton is definitely more contracted in all cases (Pt−Pt distances in the range 2.65−2.80 Å). To be noticed, in particular, is the 2.74 Å Pt−Pt separation (average) found in $\{Pt_3[\mu\text{-}P(=NBu^t)(NBu^tSiMe_3)]_3(CO)_3\}$, which is the only 42e$^-$ species supporting three PR_2-like atypical bridges.[21] Some of us have recently addressed the problem of expansion/contraction in $M_3(\mu\text{-}L_3)$ frameworks from a general structural and theoretical point of view.[22] Other geometric features of cation $\mathbf{Pt_3(CO)_3}^+$ are unexceptional and will not be further discussed in detail.

Preparation of $(\mathbf{Pt_6}^{2+})\mathbf{X_2}$. When $\mathbf{[Pt_3(PH)H_b}^+\mathbf{]X}$ was carbonylated in the presence of triflic acid excess (at least 6-fold), the reaction created a product other than $\mathbf{Pt_3(CO)_3}^+$. By monitoring the progress of the reaction ($^{31}P\{^1H\}$ NMR), we observed the formation of an equimolar amount of $[PBu^t_2H_2]X$ [δ_P = 24.2 ppm (s); triplet with $^1J_{PH}$ = 450 Hz in the proton-coupled spectrum], together with the evolution of molecular hydrogen and the formation of a new species (eq 3 and path e). This product was shown by X-ray crystallography (see below) to be the hexanuclear species $[Pt_6(\mu\text{-}PBu^t_2)_4(CO)_6]X_2$, $\mathbf{(Pt_6}^{2+}\mathbf{)X_2}$.

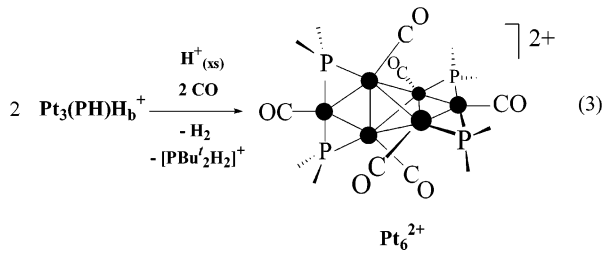

(3)

Remarkably, no trace was found of $\mathbf{Pt_3(CO)_3}^+$ and/or $\mathbf{Pt_3(CO)H_b}^+$ cations, while species $\mathbf{Pt_6}^{2+}$ does not form when a solution of $[Pt_3(CO)_3]X$ was treated with an excess of triflic acid under CO atmosphere (precluded path h).

It seemed reasonable that the protonation of the secondary phosphine drives the reaction toward the formation of the intermediate cation $\mathbf{Pt_3(CO)H_b}^+$ (three terminal CO ligands and one bridging hydride) (step f). However, the latter species, if formed, quickly dimerizes with elimination of molecular hydrogen (step g).

The solid-state structure of cation $\mathbf{Pt_6}^{2+}$ is retained in solution, as shown by its spectroscopic features. The four phosphorus centers are, in fact, equivalent since only one signal (384.1 ppm) was observed in the $^{31}P\{^1H\}$ NMR spectrum (Figure 2).

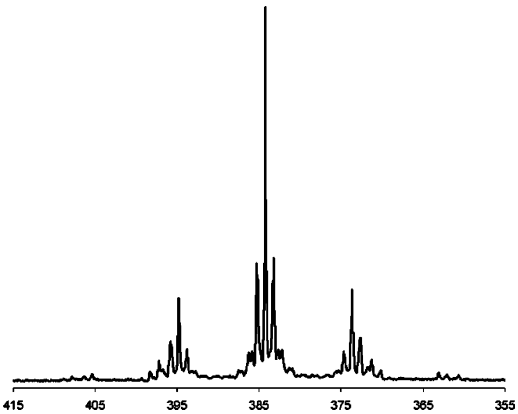

Figure 2. $^{31}P\{^1H\}$ NMR (acetone-d_6, 298 K) of $\mathbf{(Pt_6}^{2+}\mathbf{)X_2}$.

The signal consists of a central singlet (four equivalent P nuclei) flanked by satellites due to ^{195}Pt (I = $^1/_2$, natural abundance (NA) = 33.8%) containing isotopomers. The *tert*-butyl protons give a virtual triplet[23] at 1.47 ppm ($^3J_{PH}$ + $^5J_{PH}$ = 8 Hz) in the ^1H NMR spectrum due to the P−Pt−P angle close to 180° [160.7(21)°], and four signals were observed in the $^{13}C\{^1H\}$ NMR spectrum at 32.3 (*C*H$_3$), 48.5 (P*C*), 185.8 (2 *C*O), and 206.1 (4 *C*O) ppm. In the $^{195}Pt\{^1H\}$ NMR spectrum (Figure 3), a signal at −3202.8 ppm, assigned to the four inner Pt centers, is predictably very complex.

In fact, $\mathbf{Pt_6}^{2+}$ is constituted by 22 groups of nonequivalent isotopomers (total number: 2^6 = 64), and essentially all of the subspectra cannot be interpreted with simple first-order approximations. By contrast, another signal at −4960.7 ppm (broad quintet, J_{app} = 1719 Hz), assigned to the two apical Pt nuclei, is deceptively simple only by chance (the corresponding signal for other $Pt_6(\mu\text{-}PBu^t_2)_4(CO)_4X_2$ derivatives is more complex).[8,9] The oversimplification is due to J_{app}, which reasonably results from $^1J_{Pt1P(1,2)} \cong {}^1J_{Pt1Pt(2,3)}$.

Significant absorptions in the IR spectrum (Nujol, KBr) were found at 2086, 2074, and 2041 (ν_{CO}; two absorptions in $CHCl_3$

(18) (a) Bender, R.; Braunstein, P.; Tiripicchio, A.; Tiripicchio-Camellini, M. *Angew. Chem., Int. Ed. Engl.* **1985**, *24*, 861. (b) Bender, R.; Braunstein, P.; Dedieu, A.; Ellis, P. D.; Huggins, B.; Harvey, P. D.; Sappa, E.; Tiripicchio, A. *Inorg. Chem.* **1996**, *35*, 1223.
(19) Bender, R.; Braunstein, P.; Bouaoud, S.-E.; Merabet, N.; Rouag, D.; Zanello, P.; Fontani, M. *New J. Chem.* **1999**, 1045.
(20) Allen, F. H.; Kennard, O. *Chem. Des. Autom. News* **1993**, *8*, 31 (Cambridge Structural Database, version 5.25 (update April 2004)).
(21) Scherer, O. J.; Konrad, R.; Guggolz, E.; Ziegler, M. L. *Chem. Ber.* **1985**, *118*, 1.
(22) (a) Wang, W.; Carty, A. J.; Sappa, E.; Gervasio, G.; Mealli, C.; Ienco, A.; Perez-Carreño, E. *Inorg. Chem.* **2000**, *39*, 998. (b) Mealli, C. *J. Am. Chem. Soc.* **1985**, *107*, 2245.
(23) Crabtree, R. H. *The Organometallic Chemistry of the Transition Metals*; Wiley-Interscience: New York, 2001; p 260.

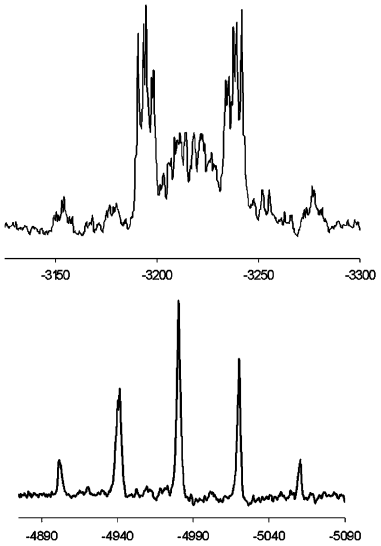

Figure 3. Resonances assigned to the inner (4 Pt, upper trace) and peripheral (2 Pt, lower trace) nuclei in the $^{195}Pt\{^{1}H\}$ NMR (acetone-d_6, 298 K) of $(\mathbf{Pt_6}^{2+})\mathbf{X}_2$.

at 2088, 2055 cm^{-1}), and at 1267, 1145, 1034, and 640 cm^{-1} (free triflate).[24]

Molecular Structure of $(\mathbf{Pt_6}^{2+})\mathbf{X}_2$. Although this structure has already appeared,[8] we highlight here full details. Crystals suitable for X-ray crystallography were obtained by recrystallization from acetone/Et_2O mixtures. A perspective view of the cation $\mathbf{Pt_6}^{2+}$ is shown in Figure 4, while the relevant bond distances and angles are presented in Table 2. Although the approximate point symmetry is as high as $\bar{4}2m$ (D_{2d}), the cluster has only one crystallographic symmetry plane. The latter coincides with the skeleton of one $[Pt_3(\mu\text{-}PBu^t_2)_2(CO)_3]^+$ fragment, namely, the one formed by atoms Pt(1), Pt(2), and Pt(3), which includes Pt(5) of the chemically equivalent fragment. The two trinuclear units are joined directly together through their unbridged Pt−Pt bonds, which are oriented perpendicularly to each other. In this manner, a tetrahedral Pt_4 core is formed.

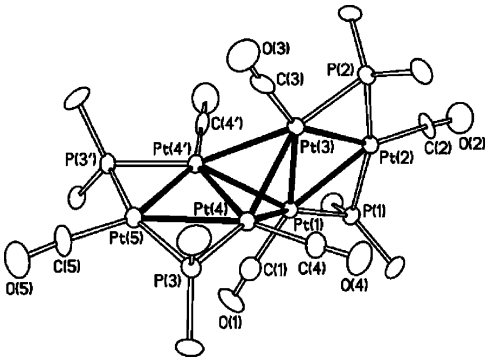

Figure 4. Molecular structure of cation $[Pt_6(\mu\text{-}PBu^t_2)_4(CO)_6]^{2+}$. The methyl groups are omitted for clarity (thermal ellipsoids at 30% probability; apex′ = x, $-y$, z).

Due to the nature of the two trinuclear components, each of the six Pt centers is coordinated by one terminal CO ligand. Also, the four external Pt−Pt bonds are still bridged through a PBu^t_2 phosphido group, while the four edges of the inner tetrahedron are unbridged. This structural arrangement is rare in the whole transition series as, besides the mixed iron−platinum cluster, $[Fe_4Pt_6(CO)_{22}]^{2-}$ (see Scheme 1),[6] the only other known examples are the hexanuclear gold clusters, $[\{(Me_3P)Au\}_6(\mu_3\text{-}O)_2](BF_4)_2$[25] and $[Au_6(dppp)_4](NO_3)_2$.[26]

Remarkably, the total number of skeletal electrons is 82 in both $\mathbf{Pt_6}^{2+}$ and $[Fe_4Pt_6(CO)_{22}]^{2-}$ (for each iron atom, only the electrons used to construct the Fe−Pt bonds are counted), but there are some noticeable differences in the Pt−Pt distances. In the present system, the Pt−Pt bonds may be distinguished into three groups. The longest ones are the four new bonds of the tetrahedral core with an average length of 2.841(1) Å. The second group consists of the PBu^t_2 bridging bonds [2.758(1) Å, average], while the two Pt1−Pt3 and Pt4−P4′ bonds, shared by the tetrahedron and each one of the triangles, are the shortest ones [2.667(1) and 2.666(1) Å, respectively]. In $[Fe_4Pt_6(CO)_{22}]^{2-}$, the four inner Pt−Pt bonds of the Pt_4 core have the longest distances [2.790(5) Å, average], but the remaining two types of bonds are essentially equal [2.680(5) Å, average]. In particular, the phosphido versus the $Fe(CO)_4$ bridge seems to determine roughly 0.1 Å elongation of the subtended Pt−Pt bond. This seems to be consistent with a stronger donor capability of the phosphido group that conveys significantly more electrons to selected Pt−Pt antibonding levels.

Noteworthy, a Pt_4 tetrahedral core is also featured by some pentanuclear platinum species. For instance, the $[Pt_3(\mu\text{-}Fe(CO)_4)_2(CO)_3]$ and $L_2Pt(\mu\text{-}CO)PtL_2$ fragments (L_2 = cyclooctadiene) add together to form four new unbridged Pt−Pt bonds[27] in $Pt_5Fe_2(CO)_{12}(COD)_2$.

Table 2. Selected Bond Distances (Å) and Angles (deg) in the Structure of $\mathbf{Pt_6}^{2+}$[a]

Pt(1)−Pt(2)	2.758(1)	Pt(3)−C(3)	1.90(3)
Pt(2)−Pt(3)	2.762(1)	Pt(4)−C(4)	1.84(2)
Pt(4)−Pt(5)	2.756(1)	Pt(5)−C(5)	1.85(3)
Pt(1)−Pt(3)	2.667(1)	Pt(1)−P(1)	2.255(6)
Pt(4)−Pt(4′)	2.666(1)	Pt(2)−P(1)	2.308(6)
Pt(1)−Pt(4)	2.841(1)	Pt(2)−P(2)	2.318(7)
Pt(3)−Pt(4)	2.841(1)	Pt(3)−P(2)	2.254(6)
Pt(1)−C(1)	1.98(3)	Pt(4)−P(3)	2.258(4)
Pt(2)−C(2)	1.86(2)	Pt(5)−P(3)	2.311(4)
Pt(1)−Pt(2)−Pt(3)	57.79(3)	P(1)−Pt(1)−Pt(2)	53.70(16)
Pt(2)−Pt(1)−Pt(3)	61.17(3)	P(1)−Pt(2)−Pt(1)	51.94(15)
Pt(1)−Pt(3)−Pt(2)	61.04(3)	Pt(1)−P(1)−Pt(2)	74.36(18)
Pt(2)−Pt(1)−Pt(4)	115.39(3)	P(2)−Pt(2)−Pt(3)	51.80(16)
Pt(2)−Pt(3)−Pt(4)	115.29(3)	P(2)−Pt(3)−Pt(2)	53.92(17)
Pt(1)−Pt(3)−Pt(4)	62.00(3)	Pt(2)−P(2)−Pt(3)	74.29(19)
Pt(3)−Pt(1)−Pt(4)	62.00(3)	P(3)−Pt(4)−Pt(5)	53.79(11)
Pt(4)−Pt(1)−Pt(4′)	55.98(3)	P(3)−Pt(5)−Pt(4)	52.02(10)
Pt(4)−Pt(3)−Pt(4′)	55.98(3)	Pt(4)−P(3)−Pt(5)	74.18(12)
Pt(1)−Pt(4)−Pt(3)	56.00(3)	P(1)−Pt(2)−P(2)	161.5(2)
Pt(1)−Pt(4)−Pt(4′)	62.010(14)	C(1)−Pt(1)−Pt(2)	154.0(8)
Pt(3)−Pt(4)−Pt(4′)	62.010(15)	C(2)−Pt(2)−Pt(1)	152.2(10)
Pt(1)−Pt(4)−Pt(5)	115.78(3)	C(2)−Pt(2)−Pt(3)	150.0(10)
Pt(3)−Pt(4)−Pt(5)	114.83(3)	C(3)−Pt(3)−Pt(2)	152.8(8)
Pt(4′)−Pt(4)−Pt(5)	61.071(15)	C(4)−Pt(4)−Pt(5)	152.4(5)
Pt(4)−Pt(5)−Pt(4′)	57.86(3)	C(5)−Pt(5)−Pt(4)	151.02(7)

[a] Symmetry transformations used to generate equivalent atoms: ′ = x, $-y$, z.

Electrochemical Study

Figure 5 shows the cyclic voltammetric profile exhibited by $\mathbf{Pt_6}^{2+}$ in CH_2Cl_2 solution. It can be observed that two separate

(24) Johnstone, D. H.; Shriver, D. F. *Inorg. Chem.* **1993**, *32*, 1045.

(25) Angermaier, K.; Schmidbaur, H. *Inorg. Chem.* **1994**, *33*, 2069.

(26) van der Velden, J. W. A.; Bour, J. J.; Steggerda, J. J.; Beurskens, P. T.; Roseboom, M.; Noordik, J. H. *Inorg. Chem.* **1982**, *21*, 4321.

(27) Adams, R. D.; Arafa, I.; Chen, G.; Lii, J.-C.; Wang, J.-C. *Organometallics* **1990**, *9*, 2350.

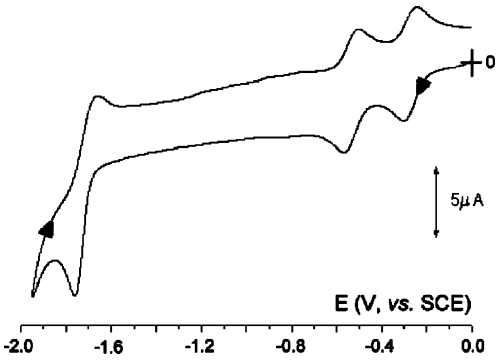

Figure 5. Cyclic voltammetric response recorded with a platinum electrode in CH_2Cl_2 solution of $[Pt_6(\mu\text{-}PBu^t_2)_4(CO)_6](CF_3SO_3)_2$ (0.3×10^{-3} mol dm^{-3}). $[NBu_4][PF_6]$ (0.2 mol dm^{-3}) is the supporting electrolyte. Scan rate is 0.1 V s^{-1}.

reductions with features of chemical reversibility (in the cyclic voltammetric time scale) are followed by a further, partially chemically reversible reduction process. Step-by-step-controlled potential experiments ($E_w = -0.4$ and -0.8 V) prove that each of the two first reductions involves the consumption of one electron per molecular unit. Also, the most cathodic step can be confidently assigned to a simultaneous two-electron transfer process, giving the unstable dianion, $\mathbf{Pt_6}^{2-}$.

Analysis of the cyclic voltammetric response of the first reductions, with scan rates varying between 0.02 and 1.00 V s^{-1}, confirms simple, chemically and electrochemically reversible, one-electron transfer processes.[28] In fact, the current ratio (i_{pa}/i_{pc}) is constantly equal to 1.0. Furthermore, the current function, $i_{pc}\cdot v^{-1/2}$, remains almost constant, and the peak-to-peak separation, ΔE_p, approaches the theoretical value of 59 mV.

Despite the chemical reversibility detected in the cyclic voltammetric time scale, Figure 6 indicates that minor byproducts form during a low-temperature (250 K) exhaustive electrolysis, corresponding to both the first and the second reduction. The corresponding peaks (pointed out by an asterisk) are assigned to the mono- or dichloride derivatives, which were also prepared by chemical routes (vide infra); their detailed electrochemical behavior will be described in a future paper. The formal electrode potentials for the cited electron-transfer processes are compiled in Table 3.

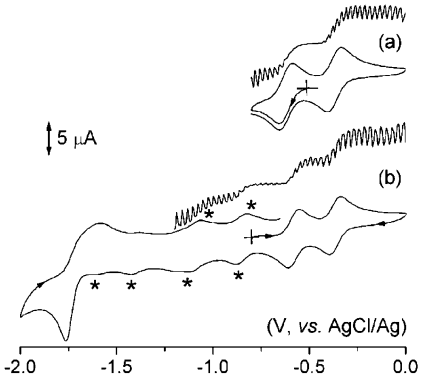

Figure 6. Cyclic (bottom) and hydrodynamic (top) voltammetric responses recorded at a platinum electrode in CH_2Cl_2 solution of $[Pt_6(\mu\text{-}PBu^t_2)_4(CO)_6](CF_3SO_3)_2$ (0.4×10^{-3} mol dm^{-3}) after (a) exhaustive one-electron reduction in correspondence of the first reduction; and (b) further exhaustive one-electron reduction in correspondence of the second reduction. $[NBu_4][PF_6]$ (0.2 mol dm^{-3}) is the supporting electrolyte. Scan rate is 0.2 V s^{-1}; T = 250 K.

Table 3. Formal Electrode Potentials (V vs SCE) and Peak-To-Peak Separations (mV) for the Redox Changes Exhibited by Dication $\mathbf{Pt_6}^{2+}$ in CH_2Cl_2 Solution

$E^{o\prime}_{(2+/+)}$	$\Delta E_p{}^a$	$E^{o\prime}_{(+/0)}$	$\Delta E_p{}^a$	$E^{o\prime}_{(0/2-)}{}^b$	$\Delta E_p{}^a$
−0.27	59	−0.54	60	−1.72	88

[a] Measured at 0.2 V s^{-1}. [b] Partially chemically reversible also in the cyclic voltammetric time scale.

It is noteworthy that the electrochemical reversibility of the 2+/+/0 sequence foreshadows, for the monocationic and the uncharged redox derivatives, essentially the same primary geometry as that of the dicationic precursor, $\mathbf{Pt_6}^{2+}$.[28] In view of the substantial chemical reversibility of the $\mathbf{Pt_6}^{2+}/\mathbf{Pt_6}^{+}$ process also in CH_2Cl_2 solution, an EPR characterization of the electrogenerated $\mathbf{Pt_6}^{+}$ has been carried out. As illustrated in Figure 7, $\mathbf{Pt_6}^{+}$ exhibits, under glassy conditions (T = 105 K), an anisotropic and axially resolved X-band EPR spectrum with metal character, for which a line shape analysis can be carried out in terms of the $S = {}^1/_2$ electron spin Hamiltonian.[29]

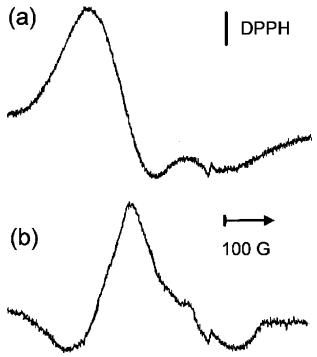

Figure 7. X-band EPR spectrum of a glassy CH_2Cl_2 solution (T = 105 K) of the electrogenerated monocation $\mathbf{6}^{+}$. (a) First derivative; (b) second derivative.

The computed EPR parameters [$g_\perp > g_{||} \neq g_{electron} = 2.0023$] and the total peak-to-peak line width [$\Delta H_{||/\perp}$: $g_\perp = 2.143(8)$; $g_{||} = 1.998(8)$; $\langle g\rangle = (g_\perp + 2g_{||})/3 = 2.092(8)$ and $a_{||/\perp}(^{195}\text{Pt}) \leq \Delta H_{||/\perp} = 210(8)$ G] account for a significant delocalization of the unpaired spin density over the whole Pt_6 metallic framework.[30,31] A composition of the SOMO based on Pt 5d orbitals with only minor contributions from the AOs of the coordinated ligands is predictable and was later confirmed by the DFT calculations. In this respect, the spectrum does not show any hyperfine splittings of the magnetically active ^{195}Pt nuclei ("satellite" splittings; ^{195}Pt $I = {}^1/_2$; NA = 33.8%) or P nuclei (^{31}P $I = {}^1/_2$; NA = 100%) or of the CO ligands. As a matter of fact, the overall experimental line width, because of the strong Pt spin−orbit coupling, overlaps largely with any possible absorption.[32] With a temperature increase to the glassy-fluid transition, the axial signal disappears and the solution becomes EPR silent.

(28) Zanello, P. *Inorganic Electrochemistry. Theory, Practice and Application*; RSC: United Kingdom, 2003.
(29) (a) Mabbs, F. E.; Collison, D. *Electron Paramagnetic Resonance of d Transition Metal Compounds*; Elsevier: New York, 1992; Vol. 16. (b) Drago, R. S. *Physical Methods for Chemists*; Saunders College Publishing: New York, 1992.
(30) Barbaro, P.; Cecconi, F.; Ghilardi, C. A.; Midollini, S.; Orlandini, A.; Fabrizi de Biani, F.; Laschi, F.; Zanello, P. *J. Chem. Soc., Dalton Trans.* **1996**, 4337.
(31) Ciani, G.; Sironi, A.; Martinengo, S.; Garlaschelli, L.; Della Pergola, R.; Zanello, P.; Laschi, F.; Masciocchi, N. *Inorg. Chem.* **2001**, *40*, 3905.
(32) Lozos, G. P.; Hofmann, B. M.; Franz, C. G. *QCPE* **1974**, *11*, 265.

Chemical Synthesis and Reversibility of Redox Derivatives. The stoichiometric stepwise reduction of cation $\mathbf{Pt_6}^{2+}$ with Cp_2Co in CD_2Cl_2 produces quantitatively the monocation $\mathbf{Pt_6}^{+}$ and the neutral derivative $\mathbf{Pt_6}$. An orange solution of $\mathbf{(Pt_6}^{2+}\mathbf{)X_2}$, treated with 1 equiv of Cp_2Co at −60 °C, turns immediately green. The IR spectrum of this solution shows the complete consumption of the cation $\mathbf{Pt_6}^{2+}$ (ν_{CO} 2088 s, 2055 s cm^{-1}) and the formation of a new species with ν_{CO} stretching absorptions shifted as expected for a greater electron density on the metal atoms (2053 s, 2018 cm^{-1}). The formation of a paramagnetic cation is confirmed by the ^1H NMR spectrum, which shows an intense broad signal at 11.7 ppm attributable to the *tert*-butyl protons of the phosphido bridges, as well as a sharp singlet at 5.8 ppm associated with the cobalticinium ion. No signals could be detected either in the $^{31}P\{^1H\}$ or the $^{195}Pt\{^1H\}$ NMR spectra, presumably due to their large broadening and the paramagnetic shift. Subsequently, the addition of 1 equiv of $[Cp_2Fe]PF_6$ to this solution causes the immediate consumption of $\mathbf{Pt_6}^{+}$ and its clean and quantitative conversion (IR, ^1H, ^{31}P, and ^{195}Pt NMR) to the starting dication $\mathbf{Pt_6}^{2+}$. Conversely, by adding, at −60 °C, another equivalent of Cp_2Co to the solution of $\mathbf{Pt_6}^{+}$ (or 2 equiv to a solution of $\mathbf{Pt_6}^{2+}$), the solution turns dark brown. After solvent evaporation, the residue was extracted with C_6D_6, and a yellow solid ($[Cp_2Co]CF_3SO_3$) was filtered off. The brown solution exhibits a further lowering of the ν_{CO} absorptions in the IR spectrum (2018, 1988, and 1975 s cm^{-1}). Moreover, the following significant NMR resonances were observed: $\delta_H = 1.40$ (virtual triplet, CC*H*$_3$), $\delta_P = 216.9$ ppm (s, with ^{195}Pt satellites, 4 equiv of P), $\delta_{Pt} = -3635.26$ (m, 4 Pt) and −5280.5 (m, 2 Pt), and $\delta_C = 203.8$, 195.4, 184.4 (s, CO), 39.6 (s, *C*CH$_3$), and 33.7 (s, C*C*H$_3$) ppm. All signals have shapes rather similar to those in the corresponding spectra of cation $\mathbf{Pt_6}^{2+}$ and of its derivatives, $Pt_6(\mu\text{-}PBu^t_2)_4(CO)_4(X)_2$ [X = halide, CHO, CCR], so far prepared.[8,9] Thus, the data are in good agreement with the formation of the neutral diamagnetic derivative $\mathbf{Pt_6}$. A discrepancy is found only in the number of IR and NMR signals observed for the CO ligands in the redox derivatives, $\mathbf{Pt_6}^{2+}$ and $\mathbf{Pt_6}$. While the former has two signals both in the IR solution spectrum and in the low-field region of the $^{13}C\{^1H\}$ NMR spectrum, $\mathbf{Pt_6}$ has an additional signal. These features are indicative of a distortion of some sort affecting the highly symmetric structure of the $\mathbf{Pt_6}^{2+}$ cluster upon the two-electron reduction. In the absence of an X-ray diffraction study, the latter structural effect has been characterized by performing DFT optimizations (see the Computational Analysis Section below).

When $\mathbf{Pt_6}$ is dissolved in CH_2Cl_2 and treated with 1 or 2 equiv of $[Cp_2Fe]PF_6$ quantitatively, immediately it is transformed into cations $\mathbf{Pt_6}^{+}$ and $\mathbf{Pt_6}^{2+}$, respectively. Solutions of complexes $\mathbf{Pt_6}^{+}$ and $\mathbf{Pt_6}$ showed behavior in the cyclic voltammograms analogous to that of their parent dication, $\mathbf{Pt_6}^{2+}$. In THF solutions, at room temperature and under inert atmosphere, $\mathbf{(Pt_6}^{+}\mathbf{)X}$ and $\mathbf{Pt_6}$ complexes remain unchanged for at least 10 h and 3 days, respectively. However, the compounds react rapidly in CH_2Cl_2 solution, giving the mono- (12 h) and dichloride (24 h) derivatives $[Pt_6(\mu\text{-}PBu^t_2)_4(CO)_5Cl]X$, $\mathbf{(Pt_6Cl}^{+}\mathbf{)X}$, and $Pt_6(\mu\text{-}PBu^t_2)_4(CO)_4Cl_2$, $\mathbf{Pt_6Cl_2}$, respectively;[9a] these can be prepared in high yield also by reacting $\mathbf{(Pt_6}^{2+}\mathbf{)X_2}$ with 1 or 2 equiv of $[n\text{-}Bu_4N]Cl$ (Scheme 3).

Scheme 3

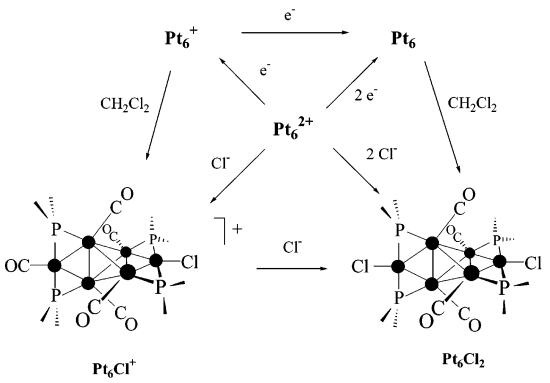

The ^1H, $^{13}C\{^1H\}$, and $^{31}P\{^1H\}$ NMR spectra of $\mathbf{(Pt_6Cl}^{+}\mathbf{)X}$ show two nonequivalent phosphide fragments ($\delta_H = 1.54$, 1.52 ppm; $\delta_C = 44.6$, 44.2 (*C*Me) and 31.7, 31.4 (*C*H$_3$) ppm; $\delta_P =$ 360.5, 348.4 ppm) indicative of the nonsymmetric substitution at the apical positions of the Pt_6 core. Accordingly, four ^{195}Pt NMR resonances at −5012.2, −3928.4, −3515.8, and −3011.9 ppm have been observed, and five ν_{CO} absorptions are present in the solution IR spectrum (2080, 2059, 2047, 2036, 2025 cm^{-1}). Due to the C_2 symmetry of cation $\mathbf{Pt_6Cl}^{+}$, the $^{13}C\{^1H\}$ NMR spectrum shows three signals at 206.0, 203.1, and 183.7 ppm for the carbon monoxide ligands. Spectral parameters for complex $\mathbf{Pt_6Cl_2}$ are given elsewhere.[9a]

Further reduction of complex $\mathbf{Pt_6}$ was attempted by reaction with $Na[C_{10}H_8]$ (1:2 molar ratio). The IR spectrum of the reaction mixture (213 K) shows that $\mathbf{Pt_6}$ is completely and readily converted, with three novel ν_{CO} absorptions being observed at 1946, 1959, and 1965 cm^{-1}, presumably due to the dianion $\mathbf{Pt_6}^{2-}$. Unfortunately, any attempt to obtain the putative $\mathbf{Pt_6}^{2-}$ derivative in the solid state failed as a consequence of its thermal instability (cf. Experimental Section).

Computational Analysis

Computational studies of the key species involved in the paths of Scheme 2, as well as the redox derivatives of the Pt hexanuclear cluster, have been performed by using the DFT B3LYP level of theory. Particularly relevant is the computed characterization of the redox derivatives, $\mathbf{Pt_6}^{+}$, $\mathbf{Pt_6}$, and $\mathbf{Pt_6}^{2-}$, in the absence of suitable X-ray structural data. For convenience, all the model compounds are indicated in italics.

Formation of $\mathbf{Pt_3(PH)H_b}^{+}$. First, a model of the starting complex $\mathbf{Pt_3H}$ (with H atoms replacing the ^{t}Bu substituents at the phosphido bridges) was optimized (see ***Pt$_3$H***). Consistently with the experimental structure of $\mathbf{Pt_3H}$,[4] the side of the Pt_3 triangle, opposite to the terminal hydride ligand, is fully opened, but the Pt−Pt, Pt−P, and Pt−C bond lengths appear somewhat

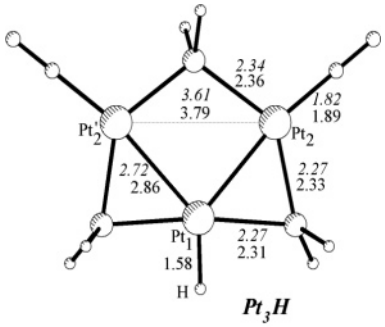

Pt$_3$H

overestimated by the calculations (the experimental parameters are in italics).

Since the *open*−*closed* dichotomy of Pt_3 triangles is a still intriguing problem,[18] an alternative model of **Pt_3H** was optimized by imposing an equilateral triangle. The energy destabilization of the system is quite small (only 2.5 kcal mol^{-1}) and shows how the cleavage/formation of metal−metal bonding in these compounds occurs over a flat potential energy surface.[33,34] Moreover, the Mulliken charges computed for the Pt_2 and Pt_2' atoms are somewhat more negative in the *closed* than in the *open* model, thus suggesting that larger electron repulsion can trigger bond cleavage. In any case, the accumulation of electron density suggests that one of the latter metals in **Pt_3H** can easily be a target of protonation. In fact, a previous study[7,15] has shown that the reaction of **Pt_3H** with triflic acid (path a) starts with the formation of the detectable hydrogen-bonded adduct Pt−CO···HX, but the actual proton transfer is to the metal. Accordingly, as a precursor of the ***$Pt_3(PH)H_b^+$*** product, the species ***1*−$Pt_3H_2^+$** features one phosphido bridge between two terminal H ligands. As shown in Scheme 4, the subsequent calculations confirm that the terminally coordinated phosphine molecule in ***$Pt_3(PH)H_b^+$*** originates from the coupling of the phosphido bridge with the pre-existing hydride ligand.[7] In fact, at the transition state (***TS***) between ***1*−$Pt_3H_2^+$** and ***$Pt_3(PH)H_b^+$***, the additional H atom has not yet switched from terminal to bridging position.

Scheme 4

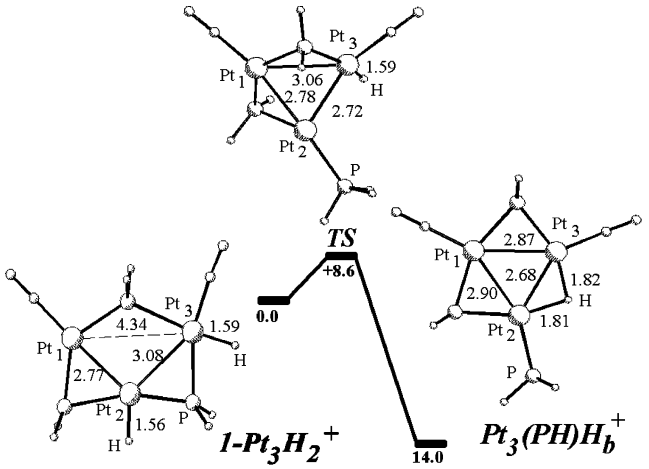

The energy barrier associated with the ***TS*** is +8.6 kcal mol^{-1}, and its surmounting causes a net stabilization energy of −22.6 kcal mol^{-1} (i.e., −14.0 kcal mol^{-1} with respect to the first protonation product ***1*−$Pt_3H_2^+$**). In agreement with the reduced number of skeletal electrons (42), the Pt_3 triangle is *closed* in ***$Pt_3(PH)H_b^+$***, and the H-bridged Pt−Pt bond is about 0.19 Å shorter than that of the other two sides, similar to the experimental analogue, $[Pt_3(\mu\text{-}PPh_2)_2(\mu\text{-}H)(PPh_3)_3]^+$, where the difference is about 0.15 Å.[35]

Two other protonation isomers were optimized, namely, ***2*−$Pt_3H_2^+$** and ***$Pt_3(H_2)^+$***. The former differs from ***1*−$Pt_3H_2^+$** only because the H and CO ligands bound to the same Pt atom are interchanged. Although ***2*−$Pt_3H_2^+$** is less stable by only 3 kcal mol^{-1}, its formation is not supported by any chemical evidence. The C_{2v} model, ***$Pt_3(H_2)^+$***, is even more stable than ***1*−$Pt_3H_2^+$** by −3.5 kcal mol^{-1}, and such a H_2 dihapto-coordinated species can be an important intermediate toward the formation of the **$Pt_3(CO)_3^+$** compound [see **$Pt_3(H_2)^+$** in Scheme 2].

Formation of $Pt_3(CO)_3^+$. The $Pt_3(\mu\text{-}PH_2)_3(CO)_3^+$ cation was optimized in D_{3h} symmetry (***$Pt_3(CO)_3^+$***, not shown). The B3LYP functional overestimates the expansion of the Pt_3 triangle [Pt−Pt sides about 0.12 Å longer than in the experimental structure of **$Pt_3(CO)_3^+$**], a fact already observed for similar electron-rich trinuclear species.[22] Attempts to optimize a transition state between ***$Pt_3(PH)H_b^+$*** and ***$Pt_3(CO)_3^+$*** (path d) or between ***$Pt_3(H_2)^+$*** and ***$Pt_3(CO)_3^+$*** (path c) were unsuccessful, but some considerations on the energies provide useful information. Recall that a key question is whether the formation of **$Pt_3(CO)_3^+$** requires necessarily the formation of **$Pt_3(PH)H_b^+$** or whether the latter is simply a stable product obtainable from the protonation of **Pt_3H** in the absence of CO (see Scheme 2). In the latter case, it cannot be excluded that the reaction of the isolated **$Pt_3(PH)H_b^+$** with CO, occurring with H_2 evolution, goes through the only computed dihydrogen species, **$Pt_3(H_2)^+$**. In this respect, the isodesmic reaction for the replacement of H_2 with a third CO ligand in ***$Pt_3(H_2)^+$*** (eq 4 and path c) is exothermic by 33.2 kcal mol^{-1}, while the substitution reaction (eq 5 and path d) involving ***$Pt_3(PH)H_b^+$*** is significantly less exothermic (24.5 kcal mol^{-1}). The difference confirms that ***$Pt_3(PH)H_b^+$*** lies in a energy minimum.

$$Pt_3(H_2)^+ + CO \rightarrow Pt_3(CO)_3^+ + H_2 \qquad (4)$$

$$Pt_3(PH)H_b^+ + CO \rightarrow Pt_3(CO)_3^+ + H_2 \qquad (5)$$

A further consideration concerns the experimentally unseen **$Pt_3(CO)H_b^+$** cluster with three terminal carbonyl ligands and one bridging hydride. The optimization of the perfectly stable ***$Pt_3(PH)H_b^+$*** model allows for the evaluation of the ***PH_3*** substitution reaction with the better π-acceptor CO ligand (path

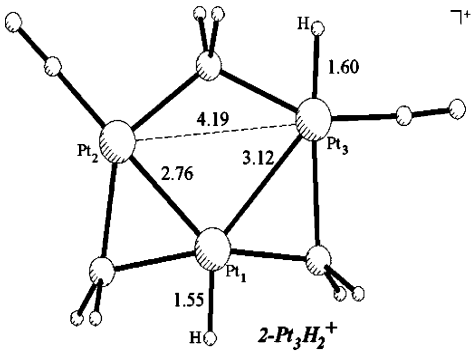

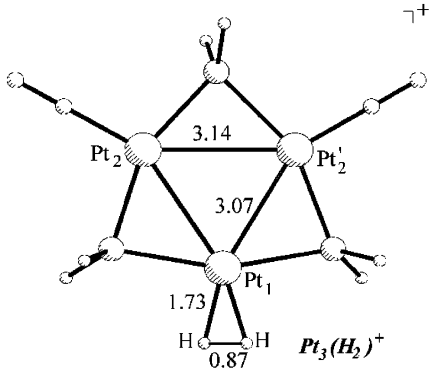

g). Since the energy balance is practically null (eq 6), it is no surprise that the formation of the thermodynamically favored product, $Pt_3(CO)_3^+$, is preferred over that of complex $Pt_3(CO)H_b^+$, which is never observed.

$$Pt_3(PH)H_b^+ + CO \rightarrow Pt_3(CO)H_b^+ + PH_3 \qquad (6)$$

When CO reacts with $\mathbf{Pt_3(PH)H_b^+}$ to give $\mathbf{Pt_3(CO)_3^+}$, H···H coupling must occur, and in this respect, the $Pt_3(H_2)^+$ model is the only H_2-containing species detected by the calculations. Thus, it is not to be excluded that, in the overall reaction leading from $\mathbf{Pt_3H}$ to $\mathbf{Pt_3(CO)_3^+}$, the undetected species, $\mathbf{Pt_3(H_2)^+}$, may be alternative to the formation of the tautomer, $\mathbf{Pt_3(PH)H_b^+}$. On the basis of the available data, it is not possible to establish which combination of paths, b + c or a + d, is preferred. While path d implies a mechanism of H_2 coupling and elimination other than that associated with metal−dihapto coordination, the hypothesis of an easy interconversion between the tautomers, $\mathbf{Pt_3(PH)H_b^+}$ and $\mathbf{Pt_3(H_2)^+}$ (paths i or a + b) would simplify the understanding of the overall reactivity pattern.

MO Architecture of the Hexanuclear Cluster, Pt_6^{2+}, and Considerations on its Formation. The optimized structure of the D_{2d} model, Pt_6^{2+}, is presented below together with the experimental geometrical parameters (in *italics*). Again, the computed Pt−Pt, Pt−P, and Pt−C distances are somewhat overestimated, but the general trends seem to be correct. The two trinuclear units lie in orthogonal symmetry planes. The most peripheral Pt atoms (Pt1 and Pt1′) define one 2-fold axis, while the other two axes intersect the pairs of orthogonal Pt−Pt edges defining the Pt_4 tetrahedral core.

For a qualitative interpretation of the bonding in Pt_6^{2+}, a diagram for the interaction between frontier orbitals of the equivalent components, $[Pt_3(\mu\text{-}PR_2)_2(CO)_3]^+$, was constructed with the help of the CACAO[36] package based on EHMO calculations[37] (see Scheme 5).

Scheme 5

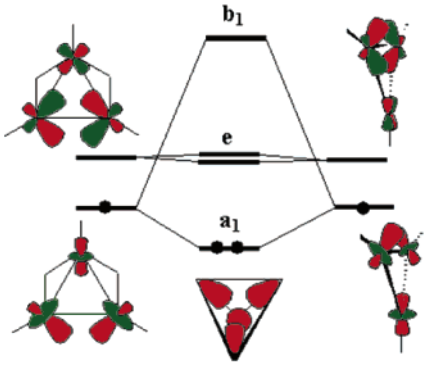

Formally, each trinuclear fragment is a radical derived from a stable complex of type $Pt_3(CO)_3^+$ upon the removal of one

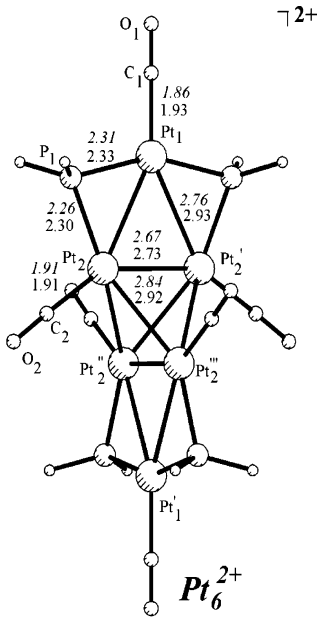

neutral PH_2 bridge. This scission leaves two out-pointing hybrids on adjacent metals, that is, those formerly used for two Pt−phosphido σ bonds. The *in-phase* and *out-of-phase* combinations of the hybrids in each fragment host only one electron. When the two units are joined together to form the inner tetrahedron, the single electrons are paired together in the stabilized HOMO a_1. Figure 8 presents a drawing of the latter (generated from the DFT coefficients), which is consistent with the previous description, although some contribution of the bridging phosphido groups is also evident.

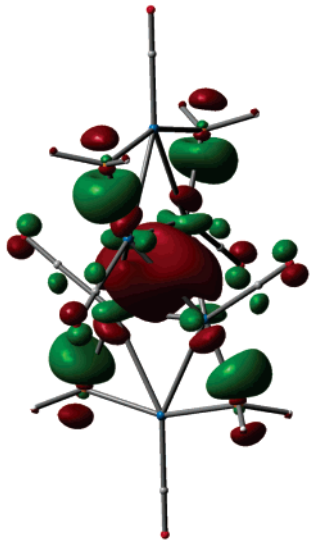

Figure 8. HOMO (a_1) of Pt_6^{2+}.

The bonding picture for the tetrahedral core corresponds to an atypical 4c-2e$^-$ model. Although two of the six tetrahedron sides are pre-existing, this can be an unusual case of three-dimensional aromaticity for transition-metal systems. In fact, the electronic arrangement has some analogies to that described

(33) We will report elsewhere a computational analysis of the Pt_3 geometry in species of the type $[Pt_3(\mu\text{-}PH_2)_3(CO_2)L]^{n+}$, where the nature of the two electron donor ligand, L, is systematically varied, including its charge (neutral or anionic). In a recent DFT study, most of the common ligands have been classified by evaluating their respective influence on three different structural or physicochemical parameters.[34] Our goal of assessing the influence of L on the trans Pt−Pt bond may represent a complementary strategy to classify the σ-donor strengths.

(34) Perrin, L.; Clot, E.; Eisenstein, O.; Loch, J.; Crabtree, R. H. *Inorg. Chem.* **2001**, *40*, 5806−5811.

(35) Bellon, P. L.; Ceriotti, A.; Demartin, F.; Longoni, G.; Heaton, B. T. *J. Chem. Soc., Dalton Trans.* **1982**, 1671.

(36) (a) Mealli, C.; Ienco, A.; Proserpio, D. M. *Book of Abstracts of the XXXIII ICCC*, Florence, Italy, 1998; p 510. (b) Mealli, C.; Proserpio, D. *J. Chem. Educ.* **1990**, *67*, 399.

(37) (a) Hoffmann, R.; Lipscomb, W. N. *J. Chem. Phys.* **1962**, *36*, 2872. (b) Hoffmann, R.; Lipscomb, W. N. *J. Chem. Phys.* **1962**, *37*, 3489.

for the T_d naked clusters, M_4^{2+} (M = Li, Na),[38] or for the C_4 skeleton of the 1,3,5,7-bisdehydroadamantane dication,[39] which are both characterized by one filled a_1 and three empty t_2 MOs. Among the certified transition-metal systems for which the electronic pattern with a filled a_1 and three empty t_2 levels applies (but not recognized as three-dimensionally aromatic), it is worth mentioning the gold clusters, $[(R_3P)Au]_4^{2+}$.[40,41] For the D_{2d} model $\boldsymbol{Pt_6^{2+}}$, the LUMOs correspond to a degenerate e set formed by these antibonding levels (see Scheme 5), which are unperturbed on dimerization due to their symmetry-imposed zero overlap. Finally, the highest level b_1 is the direct antibonding counterpart of a_1 and corresponds to the third t_2 member of the ideal Pt_4 T_d core.

Next, it is possible to make some considerations about the genesis of the hexanuclear cluster. First, the fragmentation used for the interaction diagram of Scheme 5 may not be a simple formalism due to the relative stability of the unbridged trinuclear components in some cases. In fact, the optimizations of $[Pt_3(\mu\text{-}PH_2)_2(CO)_3]^{2+,1+,0}$ (i.e., $\boldsymbol{Pt_3P_2^{2+,+,0}}$) indicate that the two cations are stationary points. In particular, the C_{2v} radical $\boldsymbol{Pt_3P_2^{+}}$ has a geometry which is not too different from that observed in $\boldsymbol{Pt_6^{2+}}$.

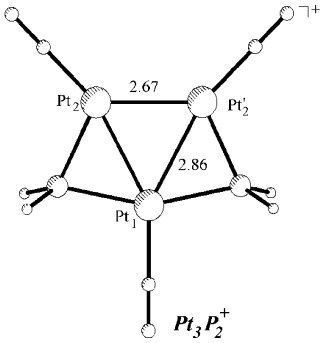

Furthermore, its SOMO and LUMO (Scheme 6) are totally consistent with those obtained at the EHMO level[37] to construct the diagram of Scheme 5.

Scheme 6

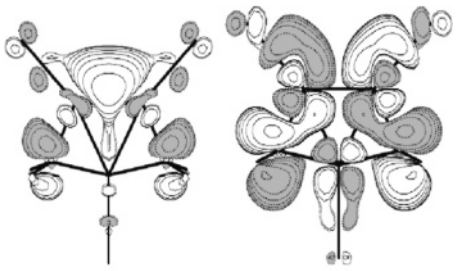

It cannot be excluded that $\mathbf{Pt_3P_2^{+}}$ has a lifetime sufficiently long to dimerize. In this case, the energy gain is calculated to be −24.7 kcal mol^{-1}. In contrast, it seems to be more improbable that $\mathbf{Pt_6^{2+}}$ originates from the coupling between the 40e$^-$ dication $\mathbf{Pt_3P_2^{2+}}$ and the uncharged species $\mathbf{Pt_3P_2}$ since the latter could not be optimized as a diamagnetic stationary point. Rather, the reduced HOMO−LUMO gap suggests a more likely triplet state in this case, but the point has not been investigated any further. As far as the formation of radical $\mathbf{Pt_3P_2^{+}}$ is concerned, the excess of triflic acid to attain $\mathbf{Pt_6^{2+}}$ (eq 6 and path e) helps to extract the terminal phosphine ligand as a phosphonium salt from $\mathbf{Pt_3(PH)H_b^{+}}$. However, before the access of the CO ligand and the formation of the undetected μ-hydride species, $\mathbf{Pt_3(CO)H_b^{+}}$ (path f), the radicals H$^\bullet$ and $\mathbf{Pt_3P_2^{+}}$ could be already split. Attempts to computationally confirm this hypothesis have been unsuccessful.

Another intriguing hypothesis on the formation of $\mathbf{Pt_6^{2+}}$ is based on the idea of the least-motion pathway for the approach of two intermediate cations of type $\mathbf{Pt_3(CO)H_b^{+}}$. Elimination of H_2 would ensue, as suggested in Scheme 7.

Scheme 7

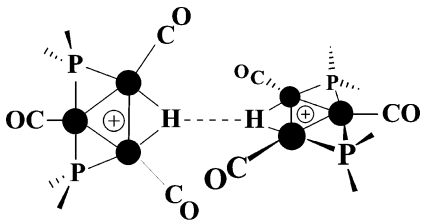

Although $H_{bridge}\cdots H_{bridge}$ attractions are rather improbable, attempts were made to mimic computationally the approach of two hydride-bridged Pt_3 units. Irrespective of the reciprocal orientation of the two $\boldsymbol{Pt_3(CO)H_b^{+}}$ models, the result is always dissociative. In any case, the energetic of the reaction, reported in eq 7, is exothermic by 29.7 kcal mol^{-1}.

$$2\ \boldsymbol{Pt_3(CO)H_b^{+}} \rightarrow \boldsymbol{Pt_6^{2+}} + \boldsymbol{H_2} \qquad (7)$$

Progressive Reduction of $\mathbf{Pt_6^{2+}}$ and Structural Effects. The hexanuclear cluster $\mathbf{Pt_6^{2+}}$ is experimentally shown to accept one or two electrons without losing the primary structure. Moreover, electrochemical techniques have shown that the $\mathbf{Pt_6^{2-}}$ dianion is temporarily formed, before being destroyed or reoxidized in a quasi-reversible process. Since none of the reduced derivatives could be studied by X-ray techniques, a series of DFT optimizations helped to elucidate the effects of the added electrons on the molecular geometry. As a matter of fact, important distortions have been observed, at variance with many clusters of high nuclearity, which act as electron sinks (the added electrons populate nonbonding metal orbitals).[42] In principle, the doubly degenerate LUMOs of the D_{2d} precursor, $\boldsymbol{Pt_6^{2+}}$ (Scheme 5), can host up to four electrons, and given the "in-triangle" antibonding nature of these MOs, expansion of the Pt_3 units could be expected. Moreover, were the D_{2d} symmetry unchanged, the two-electron-reduced species $\boldsymbol{Pt_6}$ should be

(38) Glukhovtsev, M. N.; Schleyer, P. v. R.; Stein, A. *J. Phys. Chem.* **1993**, *97*, 5541−5546.
(39) Fokin, A. A.; Kiran, B.; Bremer, M.; Yang, X.; Jiao, H.; Schleyer, P. v. R.; Schreiner, P. R. *Chem.—Eur. J.* **2000**, *6*, 1615 and references therein.
(40) (a) Zeller, E.; Beruda, H.; Schmidbaur, H. *Inorg. Chem.* **1993**, *32*, 3203. (b) Yang, Y.; Sharp, P. R. *J. Am. Chem. Soc.* **1994**, *116*, 6983.
(41) A qualitative MO analysis[36] of the gold cluster $[Au_6(dppp)_4](NO_3)_2$,[26] which has a Au_6 metal skeleton essentially equal to that of $\mathbf{Pt_6^{2+}}$, shows the non-applicability of the above aromatic electron pattern in this case. Here, the two triangular units form the central tetrahedron through a double donor−acceptor interaction between their basal Au−Au sides (the corresponding P−Au−Au−P arrangement is almost linear). Essentially, each filled Au−Au σ bonding MO interacts with the empty $p_\pi-p_\pi$ bonding combination of the orthogonally oriented Au−Au side. This gives rise to two degenerate bonding HOMOs (the symmetry is still D_{2d}), with the resulting frontier MO picture being clearly different from the $a_1 + t_2$ pattern.
(42) (a) Calderoni, F.; Demartin, F.; Fabrizi de Biani, F.; Femoni, C.; Iapalucci, M. C.; Longoni, G.; Zanello, P. *Eur. J. Inorg. Chem.* **1999**, 663. (b) Fabrizi de Biani, F.; Femoni, C.; Iapalucci, M. C.; Longoni, G.; Zanello, P.; Ceriotti, A. *Inorg. Chem.* **1999**, *38*, 3721.

paramagnetic, in evident contrast with the experimentally ascertained diamagnetism of **Pt$_6$**. Indeed, an optimized triplet model presents imaginary frequencies and was dismissed. Thus, a Jahn−Teller effect must be operative, which splits the two MO components of the frontier e set. As a matter of fact, the most reliable ***Pt$_6$***$^+$ and ***Pt$_6$*** models optimize as stationary points in D_2 symmetry.[43]

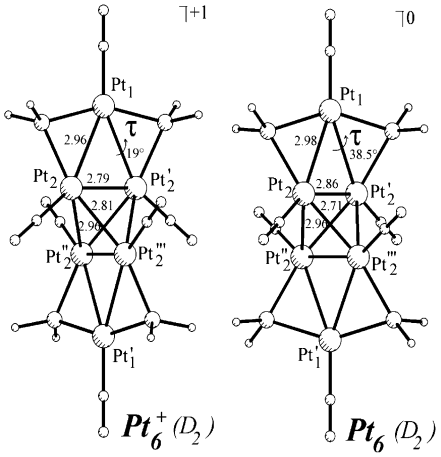

In both models, the Pt_3 skeletons are kept orthogonal, but the phosphido bridges are rotated in opposite directions. These torsions about the subtended Pt−Pt linkages (see τ in the drawings) almost double with the stepwise introduction of the electrons (from 19 to 38.5° in ***Pt$_6$***$^+$ and ***Pt$_6$***, respectively). This rearrangement seems to be the governing parameter for the stabilization of the system. The Walsh diagram of Scheme 8, computed at the EHMO level,[37] illustrates well the major electronic consequences.

Scheme 8

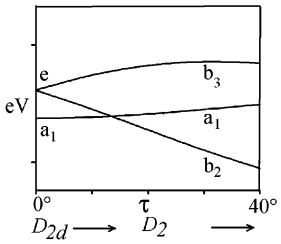

Most evident is the splitting of the initially degenerate e levels, whose components are the LUMOs of the Pt_3 units (see Schemes 5 and 6). The stabilizing MO (b_2) acquires bonding character relative to two orthogonal Pt−Pt vectors of the inner tetrahedron. The interpretation is corroborated by the systematic shortening of the Pt2−Pt2‴ and Pt2′−Pt2″ linkages from 2.92 to 2.81 to 2.71 Å in ***Pt$_6$***$^{2+}$, ***Pt$_6$***$^+$, and ***Pt$_6$***, respectively. Correspondingly, two nonadjacent bonds of the tetrahedral core become significantly localized, showing that the geometry of the latter is most affected by the added electrons. A quite similar trend was also found for the progressive reduction of the 1,3,5,7-bisdehydroadamantane dication.[39] At the EHMO level, the effect of varying only the angle τ reflects clearly on the Mulliken overlap populations of the four tetrahedral Pt−Pt bonds, which were artificially constrained to be equal. Essentially, the displacement of the PH_2 groups redirects mainly the d_π hybrids of the local L_2Pt fragments at each tetrahedral site, which overlap better pairwise. It is clear that the descending b_2 level crosses the filled level a_1 for a τ angle of about 16°. While this has no consequence if both the MOs are filled, a SOMO(b_2)−HOMO(a_1) forbidden crossing prevents an extended rearrangement of the species ***Pt$_6$***$^+$. This is most likely the reason, in the latter, the optimized value of τ is computed to be only 19°, while it increases significantly in ***Pt$_6$***.

From the computed vibrational modes of species ***Pt$_6$***$^{2+}$, ***Pt$_6$***$^+$, and ***Pt$_6$***, it has been also possible to verify that the trend associated with CO stretching frequencies are consistent with the experimental ones, namely, the progressively electron-richer metals cause larger back-donation into the carbonyls. Thus, the 0.95 scaled values of 2101 and 2061 cm^{-1}, computed for ***Pt$_6$***$^{2+}$, compare nicely with the experimental bands at 2088 and 2055 cm^{-1}. As another good match between experimental and computed values, the most energetic bands are generally assigned to the asymmetric stretching of the axial CO ligands, while the other vibrations (of e symmetry for ***Pt$_6$***$^{2+}$) are associated with the CO atoms bound to the metals of the core tetrahedron.[8] For ***Pt$_6$***$^+$, the computed frequencies are 2060 and 2025 cm^{-1} versus the experimental values of 2053 and 2018 cm^{-1}. Finally, the agreement is satisfactory also for ***Pt$_6$***, in particular, because three IR bands may be distinguished, although two of them are almost overlapping. In this case, we calculate four IR modes at 2012, 1989, 1977, and 1976 cm^{-1} which compare with the experimental data of 2018, 1988, and 1975 (overlapped) cm^{-1}, respectively. The most energetic vibration corresponds again to the asymmetric stretching of the axial CO ligands

The MO b_3, as the antibonding counterpart of b_2, increases gradually in energy since a higher level of the same symmetry mixes and mitigates the antibonding effects between the Pt2/Pt2‴ and Pt2′/Pt2″ atoms. Likely for this reason, the b_3 level can temporarily host an additional pair of electrons, so that the species **Pt$_6$**$^{2-}$ is accessible and the primary geometry of the cluster is restored if reoxidation is prompt, as occurs during the fast time scale of cyclovoltammetry. An optimization of ***Pt$_6$***$^{2-}$ in the D_2 symmetry leads to convergence with the geometric parameters, indicating that although the torsion of the phosphido bridges is only slightly increased ($\tau = 43°$) and two tetrahedral bonds are still rather short, the main effect is the expansion of the Pt_3 triangles. Also, shorter Pt−CO and longer C−O bonds, as well as some bending of the carbonyls, indicate strong back-donations as is expected for very electron-rich metals.

A computed imaginary frequency of b_1 symmetry with a rather small value (−48 cm^{-1}) indicates that the D_2 model ***Pt$_6$***$^{2-}$ is not a real minimum. Accordingly, a full optimization was attempted by eliminating all of the symmetry constraints. The system continued to oscillate for many cycles about the D_2 structure (fulfilling up to three of the four convergence criteria), and eventually the molecule disrupts with cleavage of two triangular Pt−Pt bonds (including Pt2−Pt2′ and Pt2″−Pt2‴) but a link between the two trinuclear units is maintained. After many cycles, convergence was not achieved, and the calculation was interrupted. In any case, these computational results suggest that the ***Pt$_6$***$^{2-}$ anion is a metastable species on a flat potential energy surface before a disruptive trend is started. The latter is

(43) The optimizations were actually performed in C_2 symmetry with the unique 2-fold axis coinciding with the longest molecular dimension.

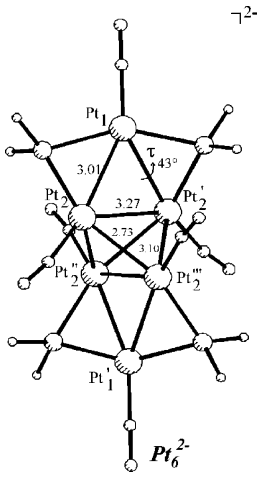

certainly imposed by the repulsion between the electron-rich Pt atoms at the tetrahedron, although the effect can be initially mitigated by the redistribution of the accumulated electron density with the Pt_3 triangles.

Conclusions

In this work, we have studied the intriguing scheme of reactions occurring between the trinuclear platinum hydride **Pt_3H** and CF_3SO_3H. As previously shown,[7,15] the reaction proceeds toward the quantitative formation of the bisphosphido-bridged **$Pt_3(PH)H_b^+$** under an inert atmosphere. A complex sequence of events, which allows the formation of **$Pt_3(PH)H_b^+$**, has been inferred from experimental findings[7] and theoretical modeling and can be summarized as follows: (i) formation of the hydrogen-bonded adduct, Pt−CO···HX; (ii) migration of the acid proton to the nearest metal center to form a terminal Pt−H bond; (iii) P−H coupling between the pre-existing hydride and the adjacent phosphido bridge to give a terminally coordinated secondary phosphine ligand; (iv) migration of the added H atom from terminal to bridging position.

Under CO atmosphere, the reaction between **Pt_3H** and CF_3SO_3H gives two different products [i.e., the hexanuclear dication **Pt_6^{2+}** or the trisphosphido-bridged tricarbonyl **$Pt_3(CO)_3^+$**], depending on whether an excess of triflic acid is used or not. An important question, which has been addressed in the paper, is whether the species **$Pt_3(PH)H_b^+$** is really a key intermediate in the overall reaction **$Pt_3H \rightarrow Pt_3(CO)_3^+$** since **$Pt_3(CO)_3^+$** is also obtained by treating the isolated **$Pt_3(PH)H_b^+$** with CO. The theoretical analysis has shown that a Pt(η^2-H_2) complex, ***$Pt_3(H_2)^+$***, is a reasonable precursor of ***$Pt_3(CO)_3^+$*** to which its tautomer, ***$Pt_3(PH)H_b^+$***, could interconvert. Unfortunately, neither the experimental nor the theoretical data are sufficient to clarify this very important aspect of the overall mechanism.

A model of the ***Pt_6^{2+}*** cation has been satisfactorily optimized by DFT calculations, which helps to clarify the stability of these rare types of hexanuclear clusters. The aromatic-like electronic nature of the tetrahedral core, quite unusual for a transition-metal system, has been pointed out. The possible mechanisms for the formation of this dication have also been discussed. Also, **Pt_6^{2+}** shows appealing redox behavior. In cyclovoltammetry, two well separated and reversible monoelectronic reductions are observed, as well as a partially reversible bielectronic reduction to the dianion **Pt_6^{2-}**. Synthetically, the **$(Pt_6^+)X$** and **Pt_6** complexes were achieved and spectroscopically characterized as stable species, but not the dianion **Pt_6^{2-}**. With the aid of the DFT calculations, the redox derivatives are shown to maintain the same primary structure, including, at least initially, the metastable dianion ***Pt_6^{2-}***. However, the cluster does not behave as an unperturbed electron sink, but distorts progressively its primary geometry since the occupied MOs have some antibonding rather than nonbonding character.

Finally, it is worth pointing out the further potential chemical usage of **$(Pt_6^{2+})X_2$**.[8,9] In fact, the [Pt_6(μ-PBu$^t_2$)$_4$(CO)$_4$] core, besides exhibiting a remarkably high thermal and chemical stability, is capable of easy chemical transformations at the two most separated Pt metals along the longest molecular axis.[8] Accordingly, the species is a promising precursor for the construction of rigid-rod or other ordered structures with cluster units and conjugated spacers embedded in the main framework.[9] The peculiar redox properties of the precursor, **Pt_6^{2+}**, detailed in this paper may be maintained and may impart interesting properties to the new materials.

Experimental Section

General Data. The reactions were carried out under a nitrogen atmosphere by using standard Schlenk techniques. Pt$_3$(μ-PBu$^t_2$)$_3$(H)-(CO)$_2$, **Pt_3H**,[4] [Pt$_3$(μ-PBu$^t_2$)$_2$(μ-H)(PBu$^t_2$H)(CO)$_2$]X, **$[Pt_3(PH)H_b^+]X$**,[7] and [Pt$_6$(μ-PBu$^t_2$)$_4$(CO)$_6$]X$_2$, **$(Pt_6^{2+})X_2$**,[8] were prepared as previously described. Solvents were dried by conventional methods and distilled under nitrogen prior to use. IR spectra (Nujol mulls, KBr) were recorded on a Perkin-Elmer FT-IR 1725X spectrophotometer. NMR spectra were recorded on a Varian Gemini 200 BB instrument; frequencies are referenced to the residual resonances of the deuterated solvent (H, ^{13}C), 85% H_3PO_4 (^{31}P), and H_2PtCl_6 (^{195}Pt). The # symbol is used to label ^{1}H, ^{13}C, and ^{31}P peaks with ^{195}Pt satellites. Molecular hydrogen evolved during the reactions was detected by gas chromatographic analysis performed with a DANI 3200 instrument equipped with a D-SM 5A column. The materials and apparatus for electrochemistry and joint EPR spectroscopy have been described elsewhere.[44] Hydrodynamic voltammetry was carried out by the use of a platinum electrode with periodical renewal of the diffusion layer.[28,45] Unless otherwise specified, potential values are referred to the saturated calomel electrode (SCE). Under the present experimental conditions, the one-electron oxidation of ferrocene occurs at $E^{\circ\prime} = +0.39$ V.

Preparation of [Pt$_3$(μ-PBu$^t_2$)$_3$(CO)$_3$]X, [Pt$_3$(CO)$_3^+$]X. Triflic acid (75 μL, 0.84 mmol) was added to a red solution of **Pt_3H** (906 mg, 0.84 mmol) in $CHCl_3$ (15 mL) under 1 atm of carbon monoxide. The solution quickly turned yellow and was shown (^{31}P NMR) to contain only complex **$[Pt_3(PH)H_b^+]X$**. After 10 min, the color of the solution turned green, while H_2 was evolved (GC). Most of the solvent was evaporated, and Et_2O (15 mL) was added. A green solid precipitated out and was recovered by filtration, washed with Et_2O, and vacuum-dried (822 mg, 78%). Similar results were observed when a solid sample of **$[Pt_3(PH)H_b^+]X$**[7] was dissolved in $CHCl_3$ under 1 atm of carbon monoxide. Anal. Calcd for $C_{28}H_{54}F_3O_6P_3Pt_3S$: C, 26.8; H, 4.31. Found: C, 26.4; H, 4.23. Neglecting the absorptions due to the different anions, we observed that IR and NMR spectra were identical to the corresponding spectra observed for [Pt$_3$(μ-PBu$^t_2$)$_3$(CO)$_3$]PF$_6$.[5] ^{31}P{^{1}H} NMR (acetone-d_6, 293 K): δ (ppm) 159.1[#] (s). ^{13}C{^{1}H} NMR ($CDCl_3$, 293 K): δ (ppm) 171.1[#] (s, $^1J_{CPt} = 2111$ Hz, $^2J_{CPt} = 92$ Hz), 41.1[#] (d, $J_{CP} = 16$ Hz, $J_{CPt} = 11$ Hz, P*C*), 33.5 (s, *C*H$_3$). ^{1}H NMR: δ (ppm) 1.37 (virtual triplet, $^3J_{HP} + {}^5J_{HP} = 7$ Hz). ^{195}Pt{^{1}H} NMR: δ (ppm) −5954 (m). IR (Nujol, KBr): 2095, 2035 (ν_{CO}), 1267, 1145, 1035, 640 (CF_3SO_3) cm^{-1}. IR ($CHCl_3$, CaF_2): 2064 (ν_{CO}).

(44) Zanello, P.; Laschi, F.; Fontani, M.; Mealli, C.; Ienco, A.; Tang, K.; Jin, X.; Li, L. *J. Chem. Soc., Dalton Trans.* **1999**, 965.
(45) Farnia, G.; Roffia, S. *J. Electroanal. Chem.* **1981**, *122*, 347.

Preparation of $[Pt_6(\mu\text{-}PBu^t_2)_4(CO)_6]X_2$, $(Pt_6^{2+})X_2$. Triflic acid (99 μL, 1.12 mmol) was added to a red solution of **Pt_3H** (151 mg, 0.14 mmol) in $CHCl_3$ (5 mL). The solution quickly turned yellow; after 30 min, the flask was filled with CO (1 atm) and the solution turned back to red in a few minutes, while H_2 was evolved (GC). The solvent was evaporated, and the residue was suspended in a THF/Et_2O (1/5) mixture. A red solid was isolated by filtration, washed with Et_2O, and vacuum-dried (87 mg, 56%). Anal. Calcd for $C_{40}H_{72}F_6O_{12}P_4Pt_6S_2$: C, 21.7; H, 3.27. Found: C, 21.9; H, 3.28. See text for IR and NMR spectra.

Characterization of $[Pt_6(\mu\text{-}PBu^t_2)_4(CO)_6]X$, $(Pt_6^{+})X$. A CD_2Cl_2 solution (0.47 mL, 0.053 M) of Cp_2Co (4.7 mg, 0.025 mmol) was added at −60 °C to an orange CD_2Cl_2 (1.5 mL) solution of **$(Pt_6^{2+})X_2$** (55 mg, 0.025 mmol). The color of the solution quickly turned green. IR (CD_2Cl_2): 2053 s, 2018 s (ν_{CO}) cm^{-1}. ^1H NMR (CD_2Cl_2, 213 K): δ 11.7 (br s, CCH_3), 5.8 (s, C_5H_5 of Cp_2Co).

When we added, at −60 °C, 8.3 mg of $[Cp_2Fe]PF_6$ (0.025 mmol) to a green solution prepared as above, the color quickly turned orange, and solution IR and ^1H, $^{31}P\{^1H\}$, and $^{195}Pt\{^1H\}$ NMR spectra exhibited only the signals of the **Pt_6^{2+}** and PF_6^- ions and of Cp_2Fe.

Characterization of $Pt_6(\mu\text{-}PBu^t_2)_4(CO)_6$, Pt$_6$. A CD_2Cl_2 solution (0.47 mL, 0.053 M) of Cp_2Co (4.7 mg, 0.025 mmol) was added at −60 °C to a green solution obtained as described above. The solution, which quickly turned dark brown, was rapidly warmed to 0 °C, and the solvent was removed in vacuo. The residue was suspended in C_6D_6 (2 mL), and a yellow solid (8.0 mg) was filtered off and identified as [Cp_2Co]X [IR (Nujol) 3120, 1420, 1050, 1000, 810 cm^{-1}; ^1H NMR (CD_2Cl_2): δ 5.8 ppm (s, C_5H_5)].[46] The IR and NMR spectra of the resulting solution gave the following data. IR (C_6D_6): 2018 s, 1988 s, 1975 s (ν_{CO}) cm^{-1}. ^1H NMR (C_6D_6, 273 K): δ (ppm) 1.40 (virtual t, $^3J_{HP} + {}^5J_{HP} = 7.2$ Hz, CCH_3). $^{13}C\{^1H\}$ NMR (C_6D_6, 273 K): δ (ppm) 203.8, 195.8, 184.4 (s, *C*O), 39.6 (s, *C*CH$_3$), 33.7 (s, C*C*H$_3$). $^{31}P\{^1H\}$ NMR (C_6D_6, 273 K): δ (ppm) 216.9[#] (s, 4 P_μ). $^{195}Pt\{^1H\}$ NMR (C_6D_6, 273 K): δ (ppm) −3635.2 (m, 4 Pt), −5280.5 (m, 2 Pt).

Identical results were obtained by adding at −60 °C a CD_2Cl_2 solution (0.94 mL, 0.053 M) of Cp_2Co (9.4 mg, 0.05 mmol) to an orange CD_2Cl_2 (1.5 mL) solution of **$(Pt_6^{2+})X_2$** (55 mg, 0.025 mmol). By adding, at −60 °C, 8.3 mg of $[Cp_2Fe]PF_6$ (0.025 mmol) to a brown solution prepared as described above, the color quickly turned green, and solution IR and ^1H NMR spectra exhibited only the signals of **Pt_6^{+}**, PF_6^-, and Cp_2Fe. The addition of a further equivalent of $[Cp_2Fe]PF_6$ caused the quick formation of an orange solution showing only the signals of **Pt_6^{2+}**, PF_6^-, and Cp_2Fe.

Preparation of $[Pt_6(\mu\text{-}PBu^t_2)_4(CO)_5Cl]X$, $(Pt_6Cl^{+})X$. *n*-Bu_4NCl (31.4 mg, 0.113 mmol) was added to a red solution of complex **$(Pt_6^{2+})X_2$** (250 mg, 0.113 mmol) in CH_2Cl_2 (5 mL). After a few minutes, all the volatiles were removed in vacuo, and the resulting red residue was extracted with acetone to give **$(Pt_6Cl^{+})X$** (216 mg, 92%; after chromatography on Celite, acetone/Et_2O 5/1 as the eluent). Anal. Calcd for $C_{38}H_{72}ClF_3O_8P_4Pt_6S$: C, 22.0; H, 3.50. Found: C, 22.1; H, 3.46. $^{31}P\{^1H\}$ NMR ($CDCl_3$, 25 °C): δ 360.5[#] (s), 348.4[#] (s). ^1H NMR ($CDCl_3$, 25 °C): δ 1.54 (vt, $^3J_{HP} + {}^5J_{HP} = 7.6$ Hz), 1.52 (vt, $^3J_{HP} + {}^5J_{HP} = 8.3$ Hz). $^{13}C\{^1H\}$ NMR ($CDCl_3$, 25 °C): δ 206.0[#], 203.1[#], 183.7[#] (s, CO), 44.6, 44.2 (P*C*), 31.7, 31.4 (*C*H$_3$). $^{195}Pt\{^1H\}$ NMR ($CDCl_3$, 25 °C): δ −5012.2 (m, 1 Pt), −3928.4 (m, 1 Pt), −3515.8 (m, 2 Pt), −3111.9 (m, 2 Pt). IR (CH_2Cl_2): ν_{CO} 2080, 2059, 2047, 2036, 2025 cm^{-1}.

Attempted Reduction of Complex Pt$_6$. A THF solution (ca. 0.025 M) of Na[$C_{10}H_8$] (3.5 mL, ca. 0.087 mmol) was added at 213 K to a brown CH_2Cl_2 solution (3 mL) of **Pt_6** (79 mg, 0.041 mmol). Immediately after mixing, the IR spectrum of the cold solution showed only three strong absorptions at 1946, 1959, and 1965 cm^{-1} (ν_{CO}), readily disappearing on increasing the temperature up to 298 K.

X-ray Crystallographic Studies. The diffractometric measurements were carried out by using a Bruker AXS P4 diffractometer equipped with graphite-monochromated Mo Kα radiation ($\lambda = 0.71073$ Å). All data were collected in the $\omega/2\theta$ scan mode, and three standard reflections were monitored every 97 measurements, checking for crystal decay and equipment stability. Data reduction was done by the XSCANS program.[47]

Table 4. Crystal Data and Structure Refinement for $[Pt_3(\mu\text{-}PBu^t_2)_3(CO)_3](CF_3SO_3)$, **$[Pt_3(CO)_3^{+}]X$**

empirical formula	$C_{28}H_{54}F_3O_6P_3Pt_3S$
formula weight	1253.95
crystal system	orthorhombic
space group	*Pnma* (No. 62)
a/Å	25.912(5)
b/Å	17.308(4)
c/Å]	9.044(2)
U/Å^3	4056(1)
Z	4
D_{calc}/Mg·m^{-3}	2.053
μ/mm^{-1}	10.539
No. measured	4695
No. unique [R_{int}]	3699 [0.0908]
No. parameters	180
R_1, wR_2 ($I > 2\sigma(I)$)	0.0556, 0.1120
R_1, wR_2 (all data)	0.1100, 0.1364
goodness of fit on F^2	1.030

A suitable crystal of dimensions 0.64 × 0.23 × 0.16 mm^3 was glued at the end of a glass fiber, and the unit cell parameters listed in Table 4 were calculated from the setting angles of 30 strong reflections. A set of 4695 intensity data was collected between $2.3° \le \theta \le 25.0°$ and corrected for Lorentz polarization and absorption effects (ψ-scan method). After merging of equivalent reflections ($R_{int} = [\Sigma|F_o^2 - F_o^2(\text{mean})|/\Sigma(F_o^2)] = 0.0908$), 3699 independent reflections were obtained. The structure solution was obtained by the standard direct methods in the *Pnma* space group. The mirror *m* perpendicular to b is perfectly valid for the cation $[Pt_3(CO)_3(PBu^t_2)_3]^+$, whereas if we constrain the triflate anion to conform with the mirror plane, an unreliable increase in the thermal parameters of some of its atoms is observed. The best result was obtained by refining the anion as a unit with fixed geometry and isotropic thermal parameters, statistically distributed over two partially superimposed positions, related to each other by the mirror plane. The hydrogen atoms were located in calculated positions, and in the last refinement cycle, anisotropic thermal parameters were used for non-hydrogen atoms of the cation. The final reliability factors are listed in Table 4.

The calculations were done by using the SHELXTL program[48] and some routines contained in the WINGX suite.[49] The crystal structure determination of compound **$(Pt_6^{2+})X_2$** has been already described in ref 8.

Computational Details. The model complexes reported herein were optimized at the hybrid density functional theory (DFT) using Becke's three-parameter hybrid exchange-correlation functional[50] containing the nonlocal gradient correction of Lee, Yang, and Parr[51] (B3LYP) within the Gaussian98 program.[52] For all of the fully optimized structures, calculations of vibrational frequencies were performed to confirm their nature as stationary points or transition states. Basis sets for platinum utilized the effective core potentials of Hay and Wadt[53] with the associated double-ζ valence basis functions. The basis set used for the remaining atomic species was the 6-31G, with the important addition of the polarization functions (d, p) for all atoms, including the hydrogens. Qualitative MO arguments have been developed thanks to the EHMO method[37] and the CACAO[36] package with its graphic

(46) El Murr, N. *J. Organomet. Chem.* **1976**, *112*, 189.
(47) *XSCANS*, X-ray Single-Crystal Analysis System, version 2.1; Bruker AXS Inc.: Madison, WI, 1994.
(48) Sheldrick, G. M. *SHELXTL-Plus*, version 5.03; Bruker AXS Inc.: Madison, WI, 1995.
(49) Sheldrick, G. M. *SHELXTL-Plus*, version 5.1; Bruker AXS Inc.: Madison, WI, 1997.
(50) Becke, A. D. *J. Chem. Phys.* **1993**, *98*, 5648.
(51) Lee, C.; Yang, W.; Parr, R. G. *Phys. Rev. B* **1988**, *37*, 785.

interface. The coordinates of all the optimized structures are available as Supporting Information.

Acknowledgment. Consiglio Nazionale delle Ricerche (CNR) and MIUR, Programmi di Interesse Nazionale, 2002-3, are gratefully acknowledged for financial support. P.Z. gratefully aknowledges the financial support by MIUR (PRIN 2003). The quantum-chemical calculations were carried out by exploiting the High Performance Systems of the Centro di Calcolo Interuniversitario CINECA (CNR-CINECA agreement). Thanks are due to Dr. Andrew Phillips for his critical reading of the manuscript.

(52) Frisch, M. J.; Trucks, G. W.; Schlegel, H. B.; Scuseria, G. E. M.; Robb, A.; Cheeseman, J. R.; Zakrzewski, V. G.; Montgomery, J. A., Jr.; Stratmann, R. E.; Burant, J. C.; Dapprich, S.; Millam, J. M.; Daniels, A. D.; Kudin, K. N.; Strain, M. C.; Farkas, O.; Tomasi, J.; Barone, V.; Cossi, M.; Cammi, R.; Mennucci, B.; Pomelli, C.; Adamo, C.; Clifford, S.; Ochterski, J.; Petersson, G. A.; Ayala, P. Y.; Cui, Q.; Morokuma, K.; Malick, D. K.; Rabuck, A. D.; Raghavachari, K.; Foresman, J. B.; Cioslowski, J.; Ortiz, J. V.; Stefanov, B. B.; Liu, G.; Liashenko, A.; Piskorz, P.; Komaromi, I.; Gomperts, R.; Martin, R. L.; Fox, D. J.; Keith, T.; Al-Laham, M. A.; Peng, C. Y.; Nanayakkara, A.; Gonzalez, C.; Challacombe, M.; Gill, P. M. W.; Johnson, B. G.; Chen, W.; Wong, M. W.; Andres, J. L.; Head-Gordon, M.; Replogle, E. S.; Pople, J. A. *Gaussian98*, revision A.7; Gaussian Inc.: Pittsburgh, PA, 1998.

(53) Hay, P. J.; Wadt, W. R. *J. Chem. Phys.* **1985**, *82*, 299.

Supporting Information Available: A table with the coordinates of all the computationally optimized models. X-ray crystallographic data (CIF file) for the structure of [Pt$_3$(μ-PBu$^t_2$)$_3$(CO)$_3^+$](CF$_3$SO$_3$), **[Pt$_3$(CO)$_3$]X**, which has been deposited with the Cambridge Crystallographic Data Centre with ref. no. CCDC 250021. The crystallographic data for the structure of [Pt$_6$(μ-PBu$^t_2$)$_4$(CO)$_6$](CF$_3$SO$_3$)$_2$, **(Pt$_6^{2+}$)X$_2$,** already published as a communication,[8] are deposited in the form of CIF file with ref. no. CCDC 159650. This material is available free of charge via the Internet at http://pubs.acs.org.

JA043626O